HOKKAIDO UNIVERSITY

Title	Development of Microwave Non-destructive Inspection Equipment for Outer Wall Tiles
Author(s)	ALSALEM, Hussain Nasser S
Citation	. ( ) 15550
Issue Date	2023-03-23
DOI	10.14943/doctoral.k15550
Doc URL	http://hdl.handle.net/2115/90390
Type	theses (doctoral)
File Information	Hussain_Alsalem.pdf

Instructions for use

Doctoral Dissertation

**Development of Microwave Non-destructive
Inspection Equipment for Outer Wall Tiles**

HUSSAIN ALSALEM

HOKKAIDO
U N I V E R S I T Y

December, 2022

Course of Systems Science and Informatics
Graduate School of Information Science and Technology
Hokkaido University

Doctoral Dissertation
submitted to Graduate School of Information Science and Technology,
Hokkaido University
in partial fulfillment of the requirements for the degree of
Doctor of Philosophy.

HUSSAIN ALSALEM

Dissertation Committee: Professor Takayuki Tanaka (Chief examinar)
Professor Satoshi Kanai
Professor Masahiko Onosato

Development of Microwave Non-destructive Inspection Equipment for Outer Wall Tiles*

HUSSAIN ALSALEM

Abstract

The separation of tiles from buildings degrades the aesthetic appeal of buildings and may result in structural failure. Therefore, tiles should be inspected periodically. However, manual inspections are expensive and require qualified experts. In this study, voids corresponding to tile separation were detected in a concrete specimen using non-destructive inspection based on electromagnetic wave detection. Furthermore, wave reflection models of healthy and defective tiles were created, and the effects of the void plane size on the reflection of defective tiles were considered. The correlation between the void plane size and the reflection intensity difference integral value was verified through multi-layer scanning using these models. The multi-layer scanning method (MLS) provides a qualitative and fundamental solution to this dilemma. Because it is based on multiple scans, it still has the potential to improve the quantity and location of the required scanning layers, increasing the accuracy and speed of the results. MLS was conducted on actual tiled concrete, including several sizes of voids. Comparing the simulation and experimental results showed a possibility of optimizing the number of scan layers. The ability to optimize scanning layers was demonstrated both theoretically and empirically. The aim of discovering the voids under the tiles is to avoid the tiles falling from the building, but the one responsible for the tiles falling is the strength of the adhesion. Therefore, this study presents a method in which the strength of adhesion of tiles can be predicted through the intensity of wave reflection from defective tiles.

Keywords: Electromagnetic wave resistance, Non destructive inspection, Multi-layer scanning method, Scan layer optimization, Adhesion strength.

Contents

List of Figures

List of Tables

Chapter 1

Introduction

1.1 Research background

Separating wall tiles from a building causes visual distortion of cities and, in the worst case, injuries to humans when the tiled fall. Therefore, wall tiles should be inspected periodically. However, there are hurdles to completing the inspection process, including its high cost and the need for qualified inspectors. Several studies have, therefore, been conducted aimed at improving the accuracy of the inspection, reducing costs, and increasing inspection speed. Most of these studies have focused on non-destructive inspection techniques (NDI) using electromagnetic waves (EMWs). These techniques can detect voids or cracks in concrete, and the void depth could be evaluated using the time/frequency domain network analyzer. However, this method uses complex and expensive systems. Multi-layer scanning (MLS) and the intensity of EMWs as data for analysis are radical solutions to this problem. The measuring device can be made simple, small, and easy to use by facilitating data analysis.However, the reflection strength changes between defective and healthy tiles have not been studied. We have mathematically modelled the process of reflecting the signal strength from defective and healthy tiles. This model made it possible to calculate the depth and area of the void, in addition to the adhesion strength required to remove tiles. Moreover, the possibility of improving the scanning of layers via a simulation using the mathematical model was explored.

Table 1.1: Comparison of Inspection Methods

	This Research	Percussion	ultrasonic waves	infrared radiation	X-ray	electromagnetic wave
Skills & Qualifications	unnecessary	Skills required	Qualifications required	unnecessary	Qualifications required	unnecessary
Non-contact measurement	passable	Immutable	Immutable	passable	passable	passable
Spatial resolution	15-30mm	45-90mm	45-90mm	Camera dependent	15-30mm	15-30mm
Equipment cost	low	low	Slightly higher	high	high	high
Work efficiency	◎	× (Manpower)	△	△ (Environmental dependent)	× (Safety measures)	△ (Computational complexity)

1.2   Previous research

For many reasons, such as their aesthetic appearance, ability to protect concrete, and ease of cleaning, wall tiles are widely used on the exterior facades of buildings. However, owing to incorrect installation, the relative pressure caused by environmental changes causes the expansion and contraction of tile bases and tiles owing to changes in humidity and temperature. In addition, relative stress occurs owing to the different grades of each material, and the material deteriorates with environmental changes, eventually creating a void between the cement layer and the tile. A void between the cement layer and the cement reduces the bonding strength of the tiles, eventually leading to the tiles falling off the building. Falling tiles from buildings are a safety hazard, in addition to affecting the aesthetics of buildings, and remove all the benefits of having tiles on the facade of buildings.

Traditional examination (hammer) is the most common method used to examine voids in buildings. To increase quality, speed, and accuracy, and decrease examination costs, non-destructive (NDI) examination techniques have been reported. For example, ultrasound[1][2][3] provides an accurate diagram of failure structures. However, ultrasound requires the device to be stuck in the object for scanning, dramatically increasing scanning time. Infrared thermal imaging [4][5][6] enables fast scanning.

However, the results of the diagnosis are affected by sunlight and temperature. Because of the drawbacks of these methods, they cannot replace traditional screening methods. Numerous NDI techniques using electromagnetic waves (EMWs) have been developed. These techniques [7] can detect voids or cracks in concrete [8]. Further, the void depth and thickness [9] can be evaluated using the time/frequency domain network analyzer [10][11] to calculate the position of foreign objects in the object. However, this method uses complex and expensive systems. By contrast, some methods [12][13] require prior knowledge of the void depth, which is not feasible in practice. Therefore, further, development is required for these technologies.

Some studies have focused on using the intensity of EMWs as data for analysis [14][15]. Typically, the reflected intensity distribution obtained using MLS (is compared with the reflective intensity data of non detective concrete (trend data). A comparison of the intensity of the reflection reveals that the integral difference volume can be considered a void. Therefore, the complexity of the measuring device and data processing can be simplified. Furthermore, this technique can detect

voids without the requirement of depth. In addition, it can measure the void size. However, the strength of the adhesion of the tiles to the wall is the most crucial factor in ensuring the safety of the tiles from falling [16][17]; therefore, the examination can be essential to finding this value. However, the mentioned techniques cannot e used to find this value. Table 1.1 shows a comparison of the existing and proposed methods.

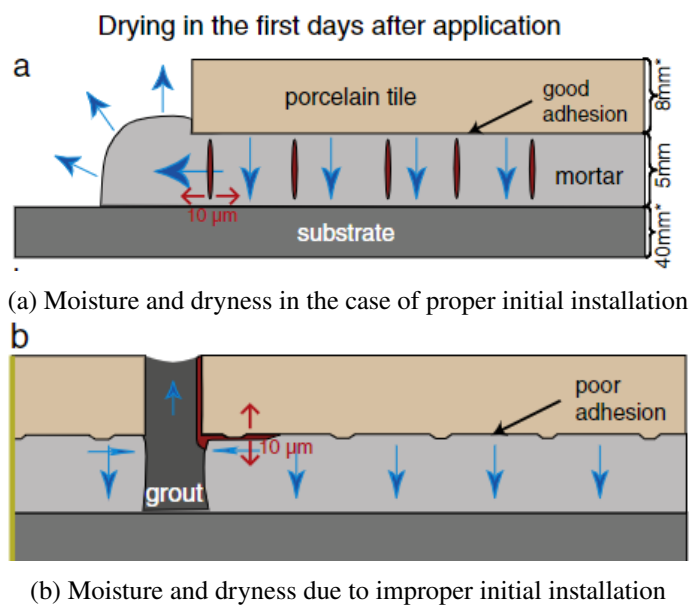

(a) Moisture and dryness in the case of proper initial installation

(b) Moisture and dryness due to improper initial installation

Figure 1.1: Effect of proper installation on tiles
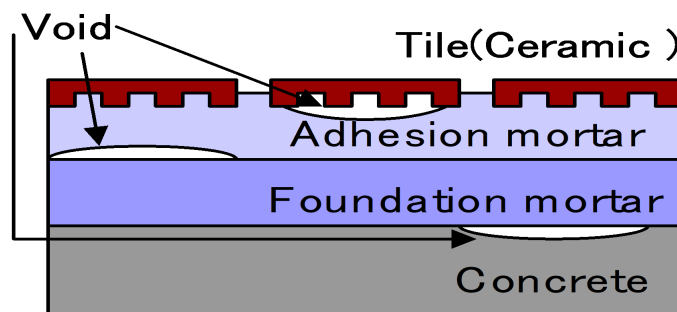

Figure 1.2: Positions of void occurrence

1.3   Purpose of this research

Natural factors, such as dryness and moisture, influence the appearance of voids under wall tiles. However, improper initial installation of tiles is a major factor in accelerating the appearance of voids. Fig.1.1a shows an example of proper initial installation of tiles, which helps the drying and moisture process. In contrast to proper installation, improper installation, which is shown in Fig.1.1b, results in the acceleration of the appearance of voids because it does not correctly help the process of water evaporation [18]. Voids usually occur under tiles, between the adhesion and foundation mortar, and between the foundation mortar and concrete (Fig.1.2) The aim of this research was divided into three objectives. The first objective was to develop a novel method for measuring the void size between wall tiles and concrete through NDI using EMWs. First, a mathematical model of the reflected waves was devised for both defective and healthy tiles. Second, a mathematical model detailing the effects of voids on the overall reflective density of defective tiles was derived. Third, an experiment was conducted using MLS on several specimens containing voids of various sizes. The experimental results revealed that the integrative value of the total reflection intensity difference changed directly with the size of the voids. Therefore, the void size can be determined using the proposed method. The second objective was to calculate the adhesive strength using the reflected strength. The third objective was to optimize the number of scanning layers required for MLS. First, experiments were conducted to detect simulated voids in concrete tiles using the MLS method. Then, based on the experimental results, a simulation was performed using a mathematical model of waves reflected from healthy and defective tiles. Finally, simulations were performed over several layers. By comparing the simulation and actual results, we demonstrate the possibility of optimizing the number of scan layers for each case.

1.4   Thesis structure

This paper explains the use of electromagnetic waves in non-destructive inspection. It is distinguished by innovative methods that make the examination devices cheaper and lighter than conventional devices. These methods include the MLS method, which is a method of scanning a sample at the same fixed X,Y point while changing the distance d_m of the antenna from the subject. This study also explains the theory of reflection of electromagnetic waves and their intensity from several layers of the sample, and a mathematical model was established based on the theory. To confirm the validity of the theory, experiments were carried out on real samples, and the test results were compared with the calculated values. This thesis consists of four chapters, which are as follows:

- Chapter 1. Focuses on the research background and previous research that was conducted using the methodology of non-destructive inspection. After that, the purpose of this study is presented.

- Chapter 2. Discusses the advantage of using electromagnetic waves for non-destructive inspection and the challenges presented by methods proposed in previous studies. It then compares then with the solution in this study. After that, the equipment used for the experiments is proposed. After that, a mathematical model of reflected waves from the healthy and defective tile is proposed. Furthermore, the relation between reflected waves and void size and adhesion strength is proved. Finally, a method for optimizing scanning layers is proposed.

- Chapter 3. Focuses on multi-layer scanning to extract voids under tiles. First, an algorithm for detecting voids is proposed. Second, an experiment is then conducted to prove the efficiency of the mathematical model. Another experiment is conducted to prove the relation between adhesion strength and reflected wave strength. Finally, an experiment is conducted to prove that the number of scanning layers can be optimized.

- Chapter 4. Estimates both the plane size and depth of voids under the tile. The theory of estimating void depth and plane size, which is based on mathematical models of reflected waves from healthy and defective tiles, is proposed. Then, an experiment is conducted on actual tiles with different void sizes and depths. Then, the measured void plane sizes and depths are compared with estimated values.

- Chapter5. Presents the conclusions and proposed future studies.

Chapter 2

Electromagnetic waves non-destructive inspection

2.1 Previous study of electromagnetic waves non-destructive inspection

Microwaves can be reflected at the boundary of different media with a medium constant (dielectric rate, magnetic rate, conductive rate). Therefore, microwaves can detect defects inside objects, and several studies have focused on using them in NDI. For example, the electromagnetic wave radar method, which is a non-destructive inspection method using electromagnetic waves, transmits a pulse wave into concrete and measures the arrival delay time of the reflected wave [19][20]. Another application is ground penetrating radar (GPR) for imaging underground buried objects such as underground buried objects (water pipes, gas pipes, communication cables, water pipes) and underground structures (stratum, underground cavity, underground water vein) [21][22][23], and ultrasound [24], which provides an accurate image of failure in structures. Infrared thermal imaging [25] has fast scanning. NDI techniques using EMWs can detect voids or cracks in concrete. Further, the void depth and thickness could be detected.

Using the intensity of EMWs as data for analysis, the reflected intensity distribution obtained using multi-layer scanning (MLS) is compared with the reflective intensity data of non detective concrete (trend data). A comparison of the intensity of the reflection reveals that the integral difference volume can be expected to be void. Therefore, the complexity of the measuring device and data processing can be simplified. Furthermore, this technique can detect voids without the requirement of depth.

All the above-mentioned methods are techniques for analyzing electromagnetic waves in the time and frequency domains. Although this method can be used to obtain a wealth of information, it requires costly instruments such as network analyzers, and the overall size of the measuring equipment is large. Furthermore, it is computationally expensive. Therefore, in this study, the frequency of the antenna was fixed to reduce the cost and weight of the measurement apparatus, and the gap was detected from the intensity information of the reflected wave, which can be detected relatively cheaply and easily.

2.2   Measurment equipment and specimen

The examination device used to detect the voids consisted of a linear actuator that directs the antenna in the x,y, and z directions. The antenna consists of a lifter, and a laser sensor that obtain the total value of the device dimension from the test sample. In the proposed method, the inspection apparatus measures the distribution of the reflected intensity at each antenna position x[mm], y[mm] by scanning the concrete surface while keeping the distance constant. Scanning is performed several times with various focal points corresponding to different heights.

2.2.1   Specimen

In this study, we used actual concreted tiles Fig 2.1a 2.1b The sample dimensions were $x = 745(mm)$, $y = 495(mm)$, and thickness= $70(mm)$. The tiles were adhered to the concrete using adhesion mortal, which is the same mortal used in actual building (Fig 2.1c). The tiles had dimensions of $x = 45(mm)$, $y = 95(mm)$, and thickness= $8(mm)$. Under the tiles, the void sheet (Fig 2.1d) was installed. This void sheet served as an alternative to voids in actual tiles and had a fixed thinness of = $8(mm)$. The shape of the void sheet was the same as that of the tile; therefore, the majored of the void sheet plate area using the percentage of the total tiles area, so we used parentage compare to the tile area.
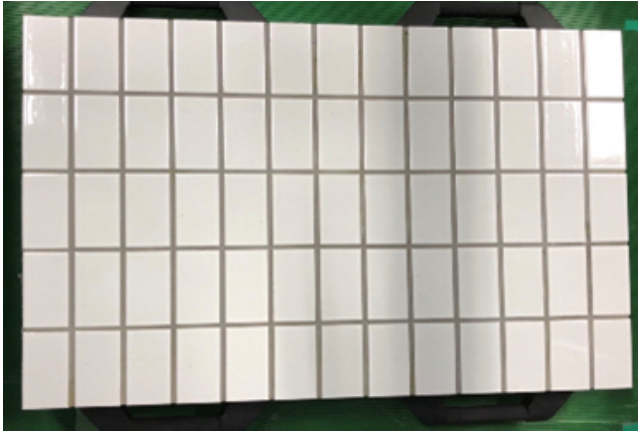
2.2.2   Micro-strip patch antenna

Fig. 2.2a shows the micro-strip patch antenna used in this study. The transmission antenna is fed by a micro-strip line, and electromagnetic waves are radiated from the patch at the tip. The radiated electromagnetic wave propagates toward the inspection object and is received by the receiving antenna after being reflected from the object. The received electromagnetic wave is detected by the receiving module and its intensity information is output. These transmitting and receiving antennae and transmitting and receiving modules are diverted from the GAP MOUSE (NEW PORTSENSORES) [26][27]. Aperture antennas such as horn antennas [28], which are excellent in directivity and sensitivity, can be cited as sensors for microwave non-destructive inspection. The resonant frequency of the microstrip antenna is a single frequency of 10 GHz. Frequency is one of the parameters that determines spatial resolution. The design dimensions of the micro-strip antenna are shown in Fig.2.3. From these dimensions, the relative permittivity ε_r of the dielectric between the patch and ground is expressed by the following equation:

$$\varepsilon_r = \left(\frac{c}{2L f_r} \right)^2 \tag{2.1}$$

where f_r is the resonant frequency of the antenna, L is the antenna length, and c is the speed of light. From Eq.2.1 $\varepsilon_e = 2.37$ The radiation pattern in the far field of the antenna is determined by calculation using the cavity model. As shown in Fig.2.4a, an x–y–z coordinate system is defined at the center of the patch.

$$E_{\phi_P}(r, \theta_P) = \frac{j k_0 W V_0 e^{j k_0 r}}{\pi r} \left\{ \sin \theta_P \frac{\sin \left(\frac{k_0 h}{2} \sin \theta_P \right)}{\frac{k_0 h}{2} \sin \theta_P} \frac{\sin \left(\frac{k_0 h}{2} \cos \theta_P \right)}{\frac{k_0 h}{2} \cos \theta_P} \right\} \tag{2.2}$$

(a) Picture of actual concreted tiles
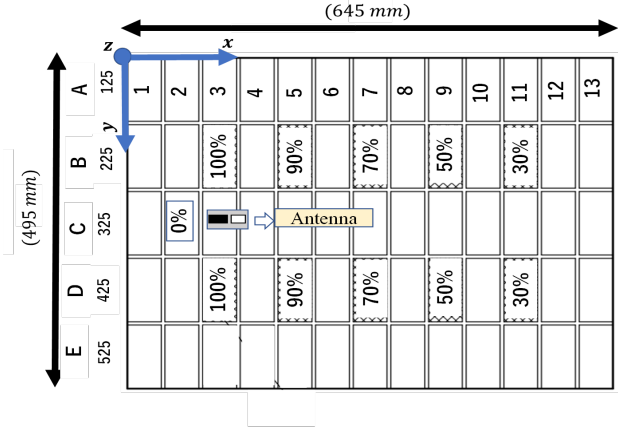
(b) Concrete dimensions, void positions, and widths.

Figure 2.1: specimen

(c) Position of the void on the side.

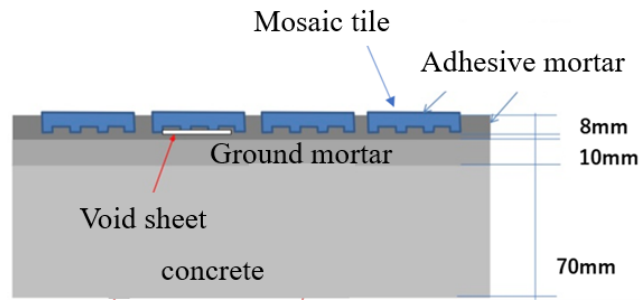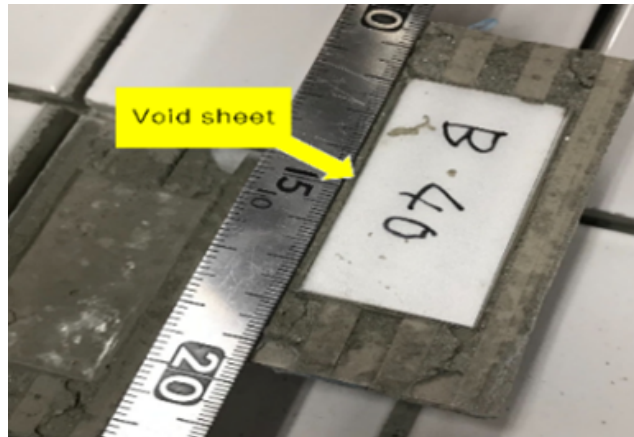(d) Void sheet material.

Figure 2.1: specimen

where r is the distance m from the center of the patch, m, V_0 is the feed voltage to the radiation slot, and λ_0, k_0 are the wavelength and wavenumber of the resonance frequency f_r in a vacuum, respectively. $E_{\phi_p}(r, \theta_p)$ denotes the ϕ direction electric field component in the $x - z$ plane $(\phi = 0°, 0° \le \theta_p \le 180°)$. Fig.2.4 shows the positional relationship and arrangement of the transmitting and receiving antennae and the test object when using the antenna. Fig.2.5 shows the radiation pattern calculated using Eq.2.2. The specification of the micro-strip antenna is shown in Table 2.1. The antennae contain a stick with a laser sensor (Fig.2.2a). The role of the laser is to detect the distance between the antenna and the object.

Table 2.1: Specifications of the micro-strip antenna

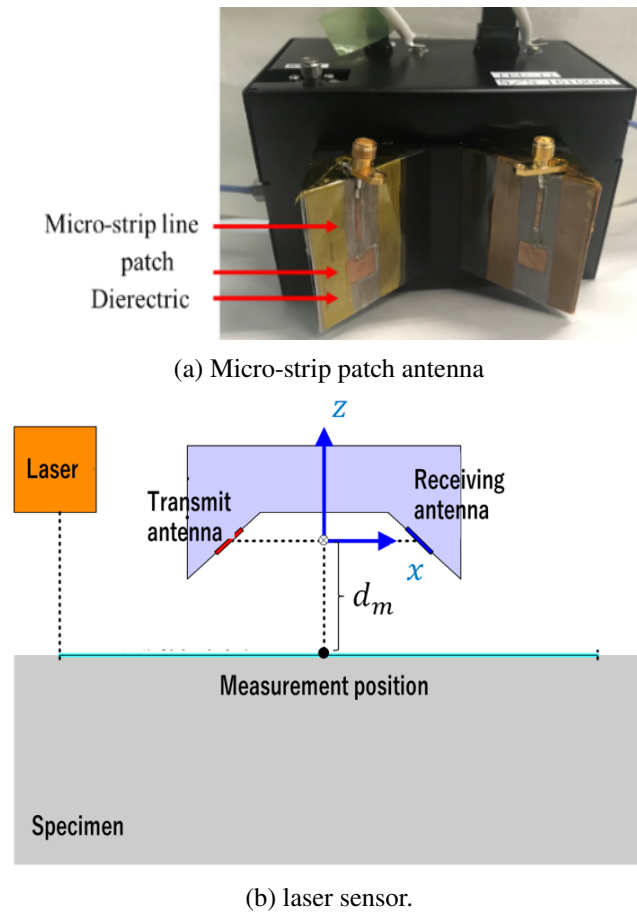| Antenna type	Single micro-strip antenna
Frequency	10 GHz
Antenna Angle	45° (From horizontal)
Distance between the receiving and transmitting antennas	50 mm

(a) Micro-strip patch antenna

(b) laser sensor.
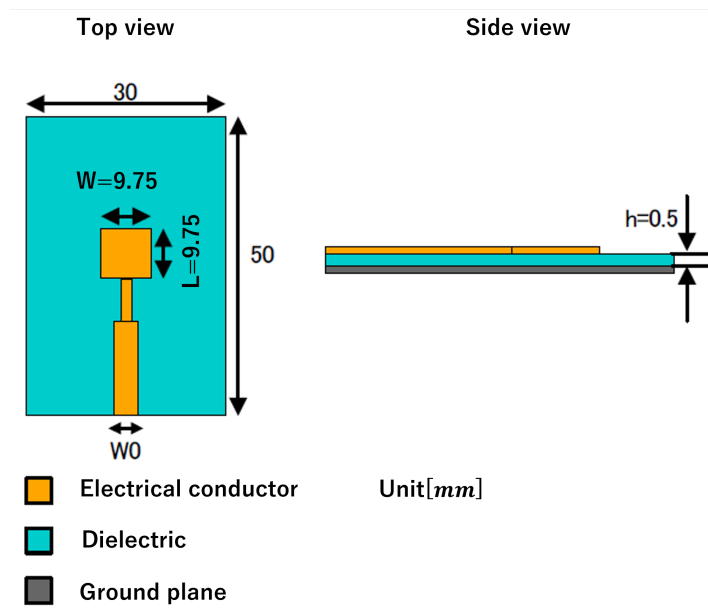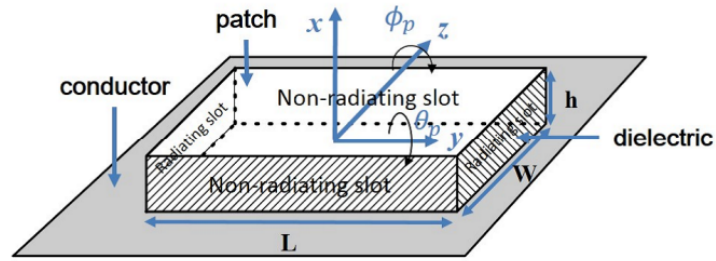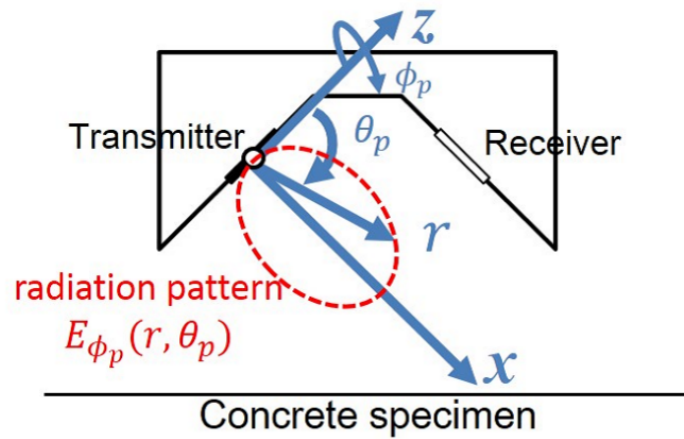
Figure 2.2: Antenna composition

Figure 2.3: Micro-strip patch antenna dimensions

(a) Overview of the cavity model

(b) Ragiation pattern of the micro-strip antenna

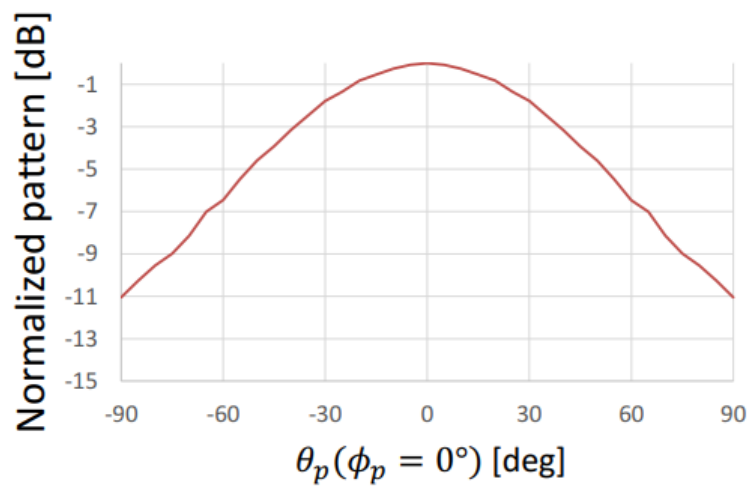Figure 2.4: Calculation of the ragiation pattern using the cavity model

Figure 2.5: Ragiation patter of the micro-strip antenna at H plane ($\phi = 0$)

2.2.3 X, Y, Z actuator

Fig 3.3 shows a microwave non-destructive inspection system using a microstrip antenna. The actuator has X, Y, and Z axis. Detection part and can move the antenna in three axial directions. Therefore, the surface of the specimen placed under the device can be scanned along the surface. This makes it possible to measure the reflection intensity distribution. The X and Y axis actuator stroke lengths are 700 mm, and that of the Z-axis is 100 mm.
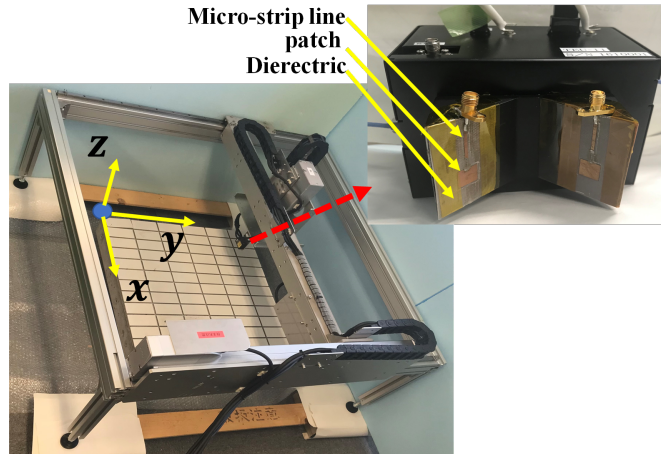

Figure 2.6: *X,Y,Z* Actuator

2.3   Definition of void plane size

The importance of knowing the size and depth of the void is that this information can be used to predict the danger of the outer tiles falling. As there is an inverse relationship between the size of the void under the tile and the tile adhesion strength, to obtain valuable information, it is important to predict the size of the void. The depth of the void is also an important piece of information for determining the adhesion strength of the tiles to the concrete. In this study, an artificial void sheet in the shape of a tile was used. Furthermore, the thickness of the void sheet in this study was constant at $1mm$. The thickness of the void sheet can be ignored because the values of d_m and the value of d_v compared to the thickness of the void sheet are considered large; therefore, the value of the thickness of the void sheet does not significantly affect the results. Fig. 2.7 shows the design of the void sheet in relation to the tiles, which have the same shape as the rectangle. The length of the sides of the void sheet is equal to the length of the sides of the tiles divided by the percentage of the designed void plane size as following equation.

$$S_v(\%) = (L_T/P) * (W_T/P) \tag{2.3}$$

where S_v is the plane area of the void sheet relative to the plane area of the tile. P is the designed percentage of the area of the void sheet. L_T is the length of tail. W_T is the width of tile.
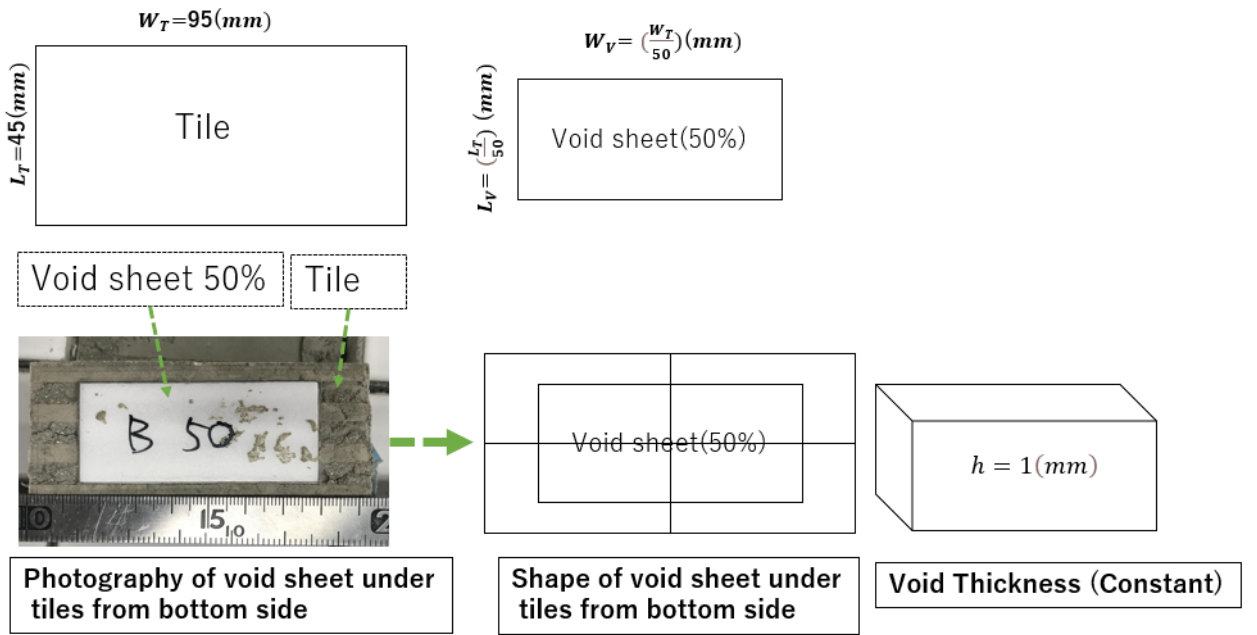
Figure 2.7: Shape, location, and area of the void sheet and the tiles

2.4   Model of the reflected wave

2.4.1   Methodology of distracting void information.

Defining the trend data theory is critical for explaining the void information extraction method. Void information can also be used to determine the effect of changing the distance d_m on the value of all the sums of the reflected waves. This feature was implemented for the healthy tiles (Fig 2.8a) and defective tiles (2.8b). We defined healthy tiles as E_T and defective tiles as E_v. The effect of d_m and d_s on E_T, and the effect of d_m and d_v on E_v are detailed in this section. Fig 2.2 presents the meaning of the symbols. Trend data can be used to estimate the EMW reflective strength of healthy tiles. The void data value is the difference between the trend data and defective tile inversion. The trend data theory is based on all the reflected waves originating from the source of the same waves. Therefore, EMW frequencies are the same but their phases differ, as displayed in Fig 2.8a. Because the reflected waves are reflected from each layer, they can be defined as E_i, which originate from E_0, and are the direct waves from the transmitting and receiving antennas. First, these waves are summarized as synthetic reflected waves E_s. The direct wave is $E_0 = E_0 sin(\omega t + k l_0)$, the reflected waves are $E_1 = E_1 sin(\omega t + k l_1)$, $E_2 = E_2 sin(\omega t + k l_2)$, and $E_3 = E_3 sin(\omega t + k l_3)$, and ω is the angular frequency of the EMWs used, k is the number of waves. l_0 is the distance between the antennas (direct wave path). Furthermore, $l_1 - l_4$ is the path of the reflected wave. The following equations summarize these results:

$$E_s = \sum_{i=1}^{4} E_i = \sum_{i=1}^{4} E_i \sin(\omega t + k l_i) \tag{2.4}$$

After the expression is expanded, the following equation is obtained:

$$E_s = E_s \sin(\omega t + \theta_s) \tag{2.5}$$

where θ_s is the phase difference of the E_s . The amplitude E_s and phase difference θ_s are given by the following equations:

$$E_s = \left\{ \sum_{i=1}^{4} E_i \cos(kl_i) \right\}^2 + \left\{ \sum_{i=1}^{4} E_i \sin(kl_i) \right\}^2 \tag{2.6}$$

$$\theta_s = \tan^{-1} \frac{E_i = \sum_{i=1}^{4} E_i \cos(kl_i)}{E_i = \sum_{i=1}^{4} E_i \sin(kl_i)} \tag{2.7}$$

d_m and d_s can affect E_t as follows:

$$l_s = 2\sqrt{(d_m + d_s)^2 + \frac{l_0^2}{2}} \tag{2.8}$$

where $\theta_s = kl_s$ and path l_s of the combined reflected wave can be calculated by dividing by number of waves k. The following equation can be expressed when calculating the trend data of healthy tiles using the following equation:

$$E_T = E_0 + E_s \tag{2.9}$$

When expanded in the same manner as the expansion from Eq2.4 to Eq2.6, the equation is transformed to the following expression:

$$E_T = E_T \sin(\omega t + \theta_T) \tag{2.10}$$

The amplitude and phase differences are as follows:

$$E_T = \sqrt{2E_0 E_s \cos(kl_0 - \theta_s) + E_s^2 + E_0^2} \tag{2.11}$$

$$\theta_T = \tan^{-1} \frac{E_0 \sin kl_0 + E_s \sin \theta_s}{E_0 \cos kl_0 + E_s \cos \theta_s} \tag{2.12}$$

d_m and d_s can affect E_T as follows:

$$l_s = 2\sqrt{(d_m + d_s)^2 + \frac{l_0^2}{2}} \tag{2.13}$$

where $\theta_s = kl_s$ and path l_s of the combined reflected wave can be calculated by dividing by number of waves k . The following equation can be expressed when calculating the trend data of healthy tiles using the following equation:

$$E_T = E_0 + E_s \tag{2.14}$$

When expanded in the same manner as the expansion from Eq2.4 to Eq2.6(refer to Appendix 2), the equation is transformed to the following expression:

$$E_T = E_T \sin(\omega t + \theta_T) \tag{2.15}$$

The amplitude and phase differences are as follows:

$$E_T = \sqrt{2E_0 E_s \cos(kl_0 - \theta_s) + E_s^2 + E_0^2} \tag{2.16}$$

$$\theta_T = \tan^{-1} \frac{E_0 \sin kl_0 + E_s \sin \theta_s}{E_0 \cos kl_0 + E_s \cos \theta_s} \tag{2.17}$$

Because $\theta_T = kl_i$, the path li of E_T , which is a composite wave of the direct waves and reflected waves, can be calculated by dividing by the wavenumbers k . Here, the amplitude E_s of the combined reflected waves is a part of the reflected direct waves E_0, and the reflection coefficient , Eq2.16 becomes

$$E_T = \sqrt{2\gamma \cos(kl_0 - \theta_s) + 1 + \gamma} \tag{2.18}$$

The value of E_T is dependent on the values of d_m and d_s because the value of l_s could be calculated using Eq2.13. This is because $\theta_s = kl_s$
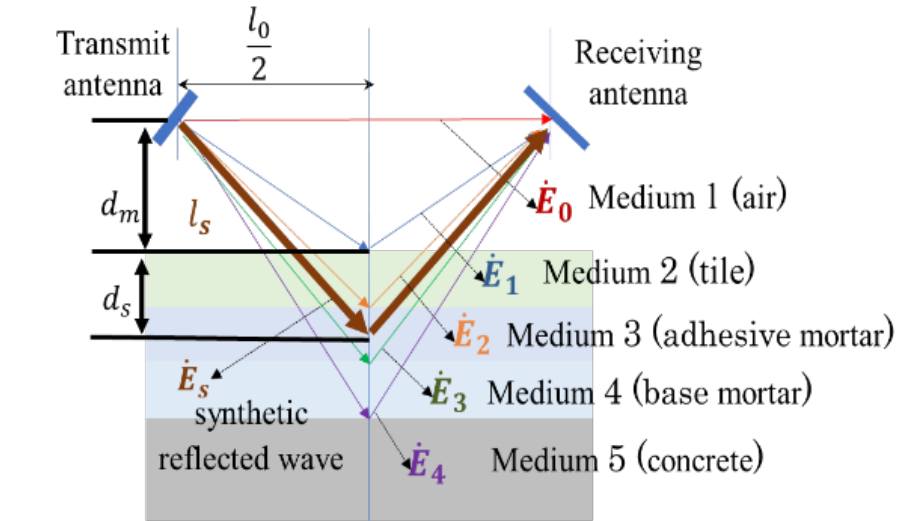
(a) Electromagnetic wave (EMW) reflection from non-detective tiles.
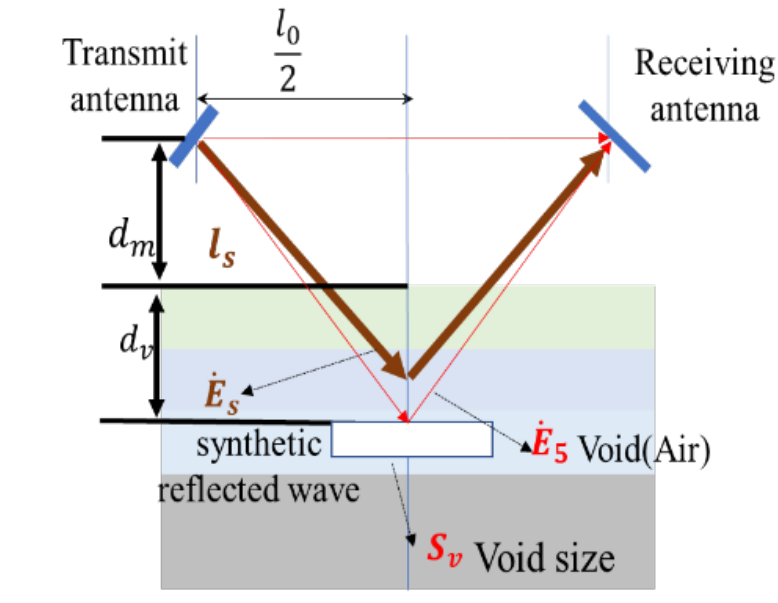
(b) EMW reflection from defective tiles.

Figure 2.8: Existing electromagnetic wave reflection transmission model

Table 2.2: Symbol meaning

symbol	Meaning
$\dot{E}_T$	Nonvoid included value
$\dot{E}_v$	Void included value
$\dot{E}_i$	The permittivity of each layer each layer's wave i
l_i	Reflection wavelength of each layer's wave i
d_m	Depth from the antenna to surface of the specimen
d_s	Depth from specimen surface to synthetic reflection
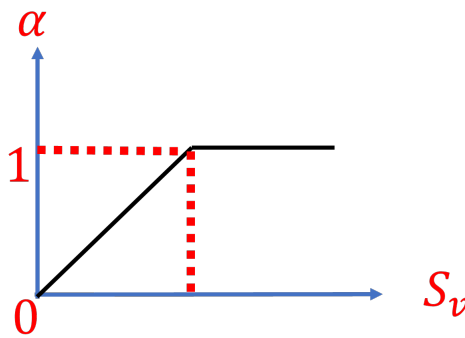
Figure 2.9: Reflected EMWs for various void sizes S_v

2.4.2 Effect of the void size on the reflected waves

In this section, the effect of void size on the reflected wave E_5 is described. Fig 2.8b displays the reflected waves from the various void sizes, S_v . In this case, the unreflected waves were ignored. The value of the waves reflected from the voids E_5 can be calculated as $E_5 = E_5 sin(\omega t + kl_5)$, and the total of the waves reflected from E_5 depends on the value of $\alpha(S_v)$. A direct relationship exists between α and S_v , a condition $0 < \alpha < 1$ exists because, if α is zero, no void exists. In addition, if $\alpha > 1$, then it represents an object with unlimited void size according to the antenna wave coverage area, as displayed in Fig 2.9.

2.4.3 Theory of defective specimen's void data

When considering the case in which an actual void exists, as displayed in Fig.2.8b, the total reflected wave from the defective specimen E_v can be calculated by adding the wave reflected from the void's reflected waves E_5 and the total reflected waves from the E_T as displayed in Eq2.18. Furthermore, the effect of void space $\alpha(S_v)$ was also included in the model. The waves that were not reflected from the voids were not considered in this model.

$$E_v = E_T + \alpha E_5 \qquad (2.19)$$

When expanded in the same manner as the expansion from Eq. 2.10 to Eq. 2.11, the equation is transformed as follows:

$$E_v = E_v + \sin(\omega t + \theta_v) \tag{2.20}$$

The amplitude and phase differences can be calculated as follows:

$$E_v = \sqrt{2E_T \alpha E_5 \cos(\theta_T - \theta_v) + (\alpha E_5)^2 + E_T^2} \tag{2.21}$$

$$\theta_v = \tan^{-1} \frac{E_T \sin \theta_T + \alpha E_5 \sin \theta_5}{E_T \cos \theta_T + \alpha E_5 \cos \theta_5} \tag{2.22}$$

where $\theta_5 = kl_5$, and the path l_5 of the combined reflected waves can be calculated by dividing by the wave numbers k . The following equation can be expressed when calculating the trend data of the tiled concrete without voids using the equation:

$$l_5 = 2\sqrt{(d_m + d_v)^2 + \frac{l_0^2}{2}} \tag{2.23}$$

the d_m and d_v has effect to the E_v.

In addition, from Eq.2.21, after using the Maclaurin series, the following equation is obtained:

$$E_v(\alpha) \approx E_T + \frac{d}{d\alpha} E_v(0)\alpha \tag{2.24}$$

E_v and α have a proportional relationship. Therefore, the relation between the void size $\alpha(S_v)$ and $P(x)$ (reflection intensity difference integral value) is assumed to have a proportional relationship.

2.5   Relation between reflectance and void plane size

The total value of the reflection intensity from the void is calculated using the Eq.2.21. The value of E_v changes based on two coefficients, S_v and d_v. This change expresses a direct relationship as explained in the equation. Therefore, S_v can be estimated[29]. Fig.2.10 shows an example of the relationship between E_5 and S_v in the case of S_v being 30% and 90% the tile area. There is a limit to this relationship, which is that the area of the void should not be greater than the coverage of the antenna.
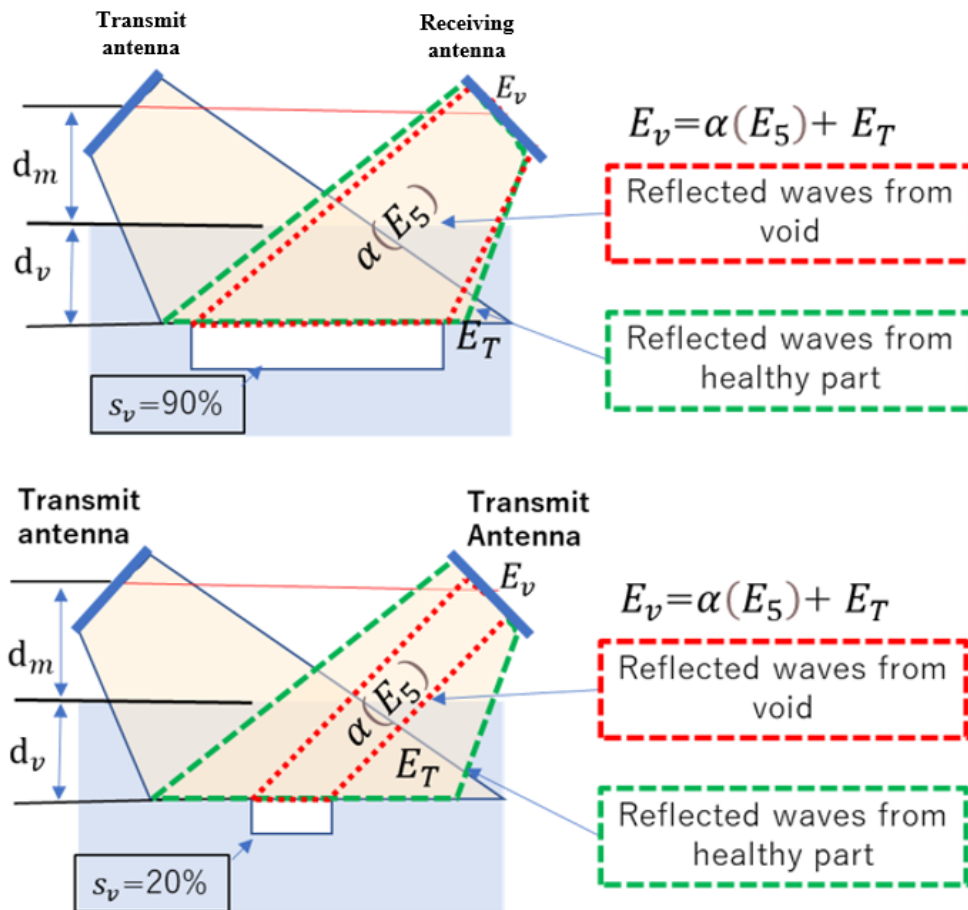

Figure 2.10: Reflected waves from S_v in the cases where of S_v is 20% and 90% of the tile area

Chapter 3

Electromagnetic wave analysis model for extracting void information

3.1 Extraction of void information using reflection intensity

The MLS method can be used to obtain the overall reflection intensity distribution. Depending on the change in d_m, the propagation path lengths of the reflected wave change, which causes various interferences and, eventually, the intensity of the obtained total reflection changes, which renders void detection possible at different d_v. The void-detection algorithm using the MLS system is displayed in Fig.3.1. First, the total reflection intensity, E_v, is measured by the MLS. Here, E_T is the intensity received in the healthy part. Next, we obtain the void data using $\Delta E(x, d_m)$. When considering Eq. 2.24, the following equation is applied:

$$\Delta E(x, d_m) = E_v - E_T = \frac{d}{d\alpha} E_v(0)\alpha \tag{3.1}$$

This is the value obtained after subtracting the normal and abnormal reflected wave data. The interference of the void-reflected wave is determined by considering the difference between the total reflection intensity and the trend reflection intensity. Finally, the result obtained by MLS scanning was comprehensively determined by the evaluation function $P(x)$, which revealed that the voids can be quantitatively detected from the measured reflected intensity. $P(x)$ can detect voids from $\Delta E(x, d_m)$ and is defined as follows:

$$\frac{1}{N} \sum_{i=1}^{N} |\Delta E(x, d_m j)| \tag{3.2}$$

where N is the number of data points along the d_m axis at each x. $d_m j$ is the number of d_m. Because $\Delta(x, d_m j)$ is obtained from the difference between the reflected intensities, it can be negative; therefore, we consider the absolute value.
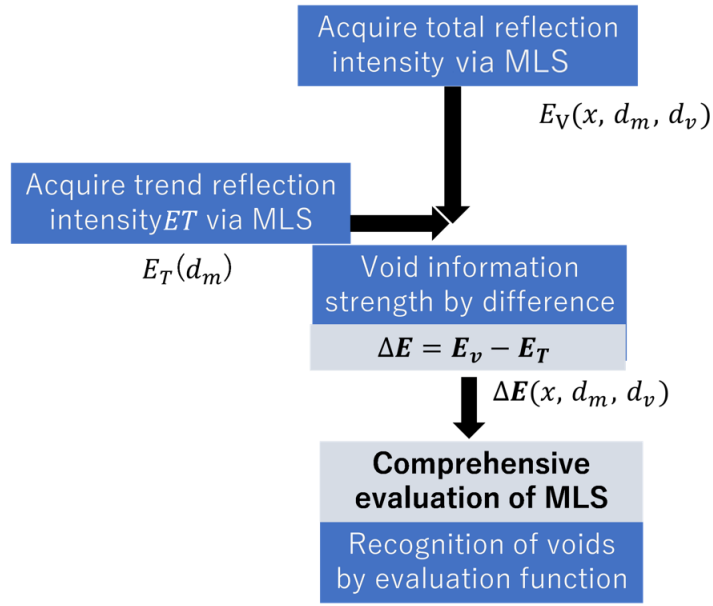
Figure 3.1: Reflected EMWs from various sizes of void S_v

3.2 Calibration to normal tiles reflection intensity

First, the value of the reflection intensity was measured from the healthy tiles. In this experiment, the positions of the healthy tiles were determined. The locations of the healthy tiles are presented in Fig.3.7. After considering the data of all the healthy tiles, calibration was conducted using Eq. 2.18. The parameter settings for $E_0, \gamma, and k$ were set to minimize the difference between $\hat{E}_T$ and E_T , as follows:

$$\min_{E_0,k} \sum_{i=1}^{N} (\hat{E}_T(x, d_m j) - E_T(x, d_m j))^2 \tag{3.3}$$

where N is the number of d_m. The same method was applied to the remaining specimens. $\hat{E}_T$ is the estimated value of the reflection intensity of the healthy tiles.

3.3 Total reflection intensity measurement by MLS

The MLS output is the sum of the difference between the reflection intensity value of a defective tile $E_v(x, d_m)$ and that of a healthy tile $E_T(x, d_m)$ at scan position x when scanning at a different distances d_m from the specimen surface to the sensor. This process is repeated for each layer number N , and the output function $P(x)$ is the mean of the sum of $\Delta E = |E_v - E_T|$ for each layer d_m for N scanning times. The advantage of the MLS methodology is that the E_v value can be calculated without prior knowledge of the d_v value. However, the value of E_v depends on the value of d_v . Therefore, the ΔE must be calculated for all layers. For further clarification, simulations were conducted using E_v and E_T obtained from the mathematical models, for $64mm \le d_m \le 74mm$,
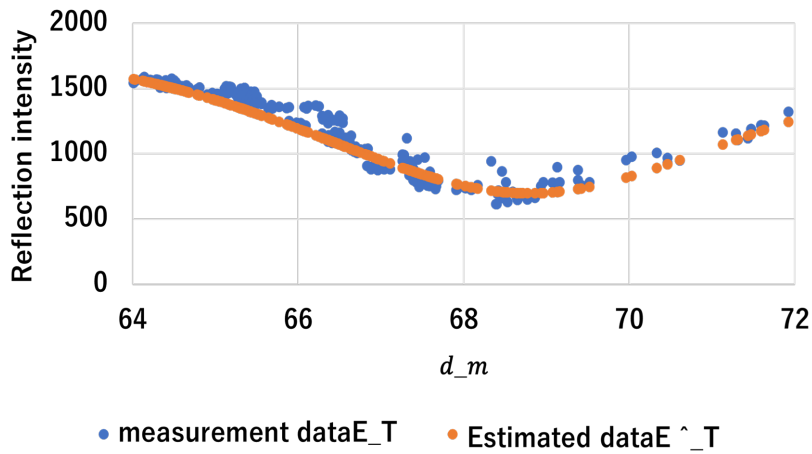
Figure 3.2: Calibration of the reflection intensity of the healthy tiles

and $d_v = 9mm$ and $10mm$. Fig.3.3a shows the values of E_v (red) and E_T (blue) for $d_v = 9mm$. At certain points $d_m = 64, 70, 71, 72, 73, and 74mm$, ΔE had a relatively more minor value than that for the rest of the layers. However, Fig.3.3b shows that E_v (red) and E_T (blue) for $d_v = 10mm$ for the points at $d_m = 64, 65, 66, 67, 73, and 74mm$ had a high value. Therefore, all points should be included when calculatingΔE.
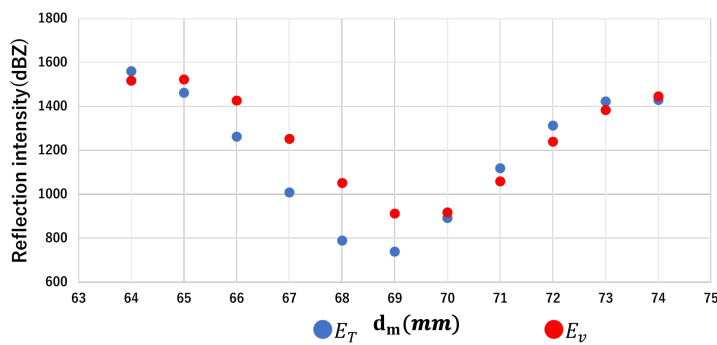
(a) Values of E_T and E_v for $d_v = 9mm$
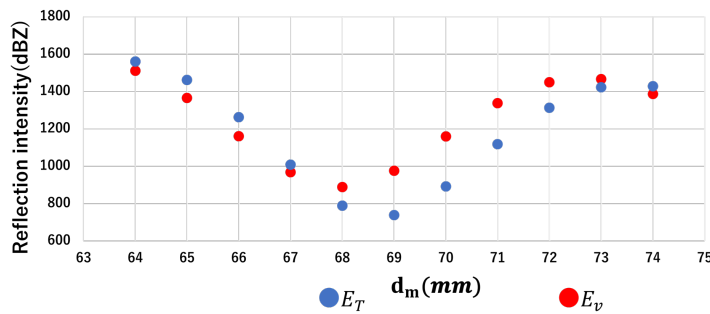
(b) Values of E_T and E_v for $d_v = 10mm$.

Figure 3.3: Values of E_T and E_v in diffrant value of d_v

3.4   Void extraction experiment and results using the models

We conducted MLS measurement experiments by using three real tiled concrete specimens. This section details the effectiveness of the proposed method for inspecting actual tiled walls. All specimens included an artificial void with various void sizes. The voids sizes and locations are shown in Fig. 3.7, and the specimen specifications are shown in Fig. 2.1 with various void sizes. MLS scanning was performed for specimens 1 B (2–12) and 1 D (2–12), specimen 2 D (2–12), and specimen 3 B (2–12), as presented in Table.3.1 . The wave reflection intensity $E_v(x, d_m j)$ was obtained by scanning along the x-axis in each scanning area nine times at $64mm \leq dm \leq 72mm$. Subsequently, the calibration of healthy tile data, such as calibrating specimen 1 B using Eq. 3.3, was conducted. The calibration results are presented in Fig.3.2. The orange color represents the measured data E_T . The calibration had an error. The average error was calculated using the following equation:

$$\frac{1}{N} | \sum_{j=1}^{N} (\hat{E}_T(x, d_m j) - E_T(x, d_m j))| \tag{3.4}$$

The average errors for the remaining specimens are presented in Table.3.2. The evaluation function $P(x)$ using this result is displayed in Figs. 3.5a, 3.5b, 3.5c, and 3.5d. The red-colored lines represent the defection information in these figures, and the yellow-colored lines are the healthy tile information. To avoid the effect of joints[31][32], the samples were considered at a distance $\pm 10mm$ from the joints. According to Table 3, the void position/size and healthy tile positions are displayed.

The results of the void size and MLS scattergram plotted in Fig.3.6 indicate that a correlation exists between the void size$\alpha(S_v)$ and reflection intensity difference integral value $P(x)$. Additionally, a linear relationship exists between the two variables. The correlation coefficient revealed a strong correlation with $R = 0.64, P < 0.05$.

3.5   Relationship between void size and adhesion strength

From the principle of an inverse relationship between the void size and the bonding strength, and as the void size between wall tiles and concrete can be measured through NDI using EMWs, the possibility of measuring the bonding strength through NDI using EMWs was imposed[30]. This hypothesis has been experimentally confirmed. First, an experiment was conducted by using MLS on several specimens containing voids of various sizes. Second, pull-off testing was conducted on the same scanned tiles to measure the bonding strength. The experimental result confirmed that the bonding strength decreases with an increase in the void size. The test results also revealed a relationship between the integrative value of the total reflection intensity difference and the bonding strength. Therefore, the void size can be determined using the proposed method.

Table 3.1: Healthy and defective tile distributions

Specimen		1		2	3
Tile number y(mm)		B 225	D 425	D 425	B 225
Tile number x(mm)					
1	(0-45)	NA	NA	NA	NA
2	(50-95)				
3	(100-145)	100%	100%	95%	
4	(150-195)				50%
5	(200-245)	90%	90%		
6	(250-295)			85%	
7	(300-345)	70%	70%		40%
8	(350-395)				
9	(400-445)	50%	50%	75%	
10	(450-495)				30%
11	(500-545)	30%	30%		
12	(550-595)			65%	
13	(600-645)	NA	NA	NA	NA

Table 3.2: Calibration results for the specimens

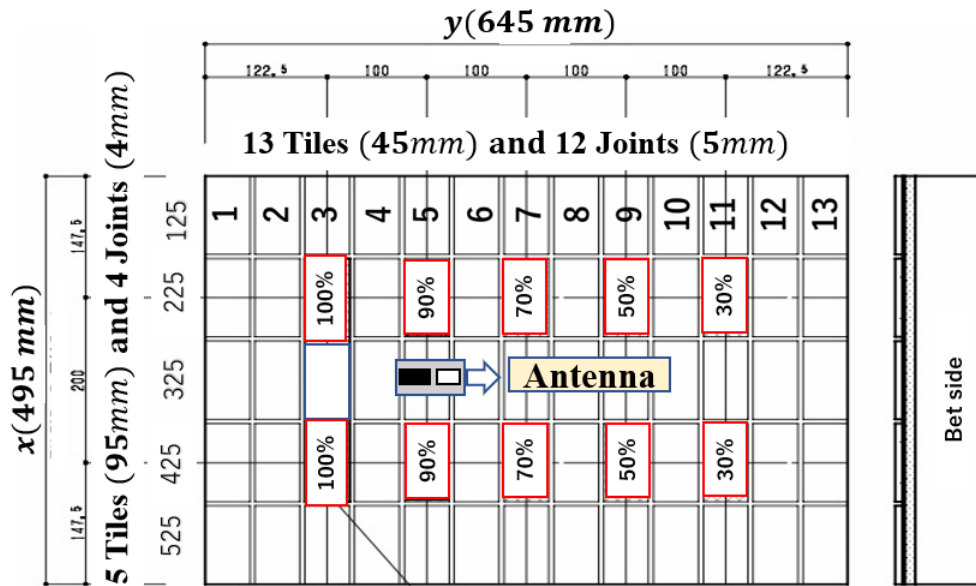| Specimen	1		2	3
	B 225	D 425	D 425	B 225
average error	103.2	72.0	87.0	98.0

Figure 3.4: Overview of the scanning of the tiled concrete.

3.6 Experiments and results for the adhesion strength and reflection strength

3.6.1 MLS measurement and result for the reflected wave strength of healthy and defective tiles

Experiments were conducted using real tiled concrete. This experiment demonstrates the effectiveness of the proposed method for inspecting actual tiled walls. The multi-layered scanning was performed at $y = 215, 225, 415, 425mm$. Intensity $E_R(x, d)$ was obtained by scanning along the x-axis in each scanning area several times at $60mm < d < 90mm$ in intervals The evaluation function $P(x)$ using this result is shown in Figs.20(a) to 20(d). The vertical axis shows the variation in the reflection intensity integrated value, according to different state void and non-void tiles. At a void size position that was a distance of $\pm10mm$ from the joints, the average integrated reflection intensity value was taken. The horizontal axis was the tile position. The red-colored tiles have voids of different sizes, from 100% to 30%. Other tiles are normal tiles with no void. For most lines, the integrated value of the reflection intensity is high for the large void size and low for the small void size, except for Line B 225 and Line B 215, for tiles No. 5 and 7, which show no changes in the value. Line D for tile No 5 also does not exhibit any changes.

3.6.2 Tile peeling test

The adhesion strength measurement was demonstrated using a manual construction research type adhesion tester (LPT-3000 Ox Jack Co., Ltd.). The design research type adhesion tester is shown in 3.9.Before using the tester, a hammering test was demonstrated to determine whether there was void or not. Fig.3.10 shows the parts of the tester. It consists of an analog load cell, a pump handle, and an attachment. When turning the pump handle clockwise, the attachment rises, and pulls the tile until it is removed (Fig.3.11). At the same moment the tile is removed, the power consumed to remove the tile measured by the analog load cell and recorded. The recorded data is shown in
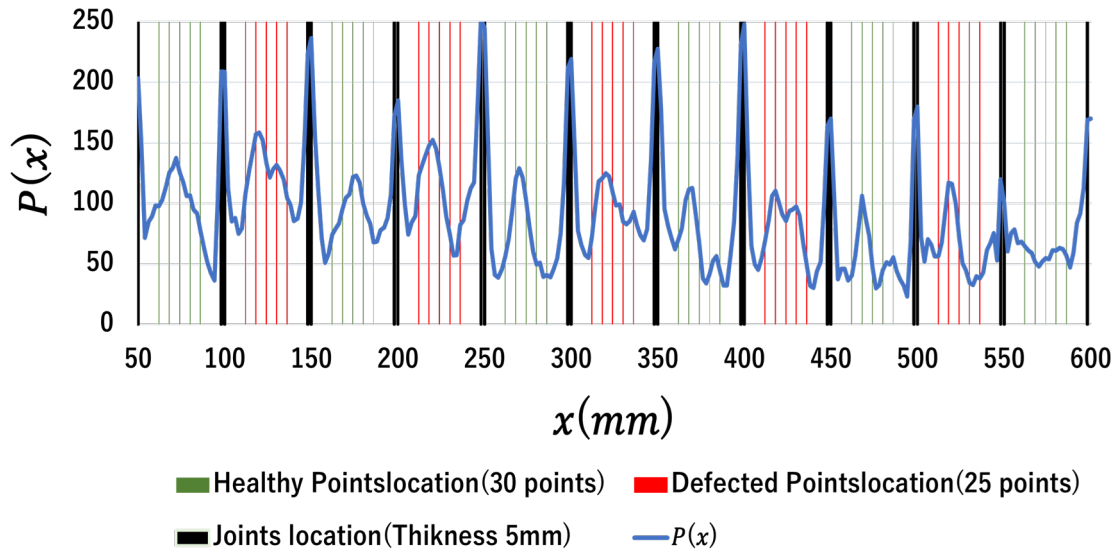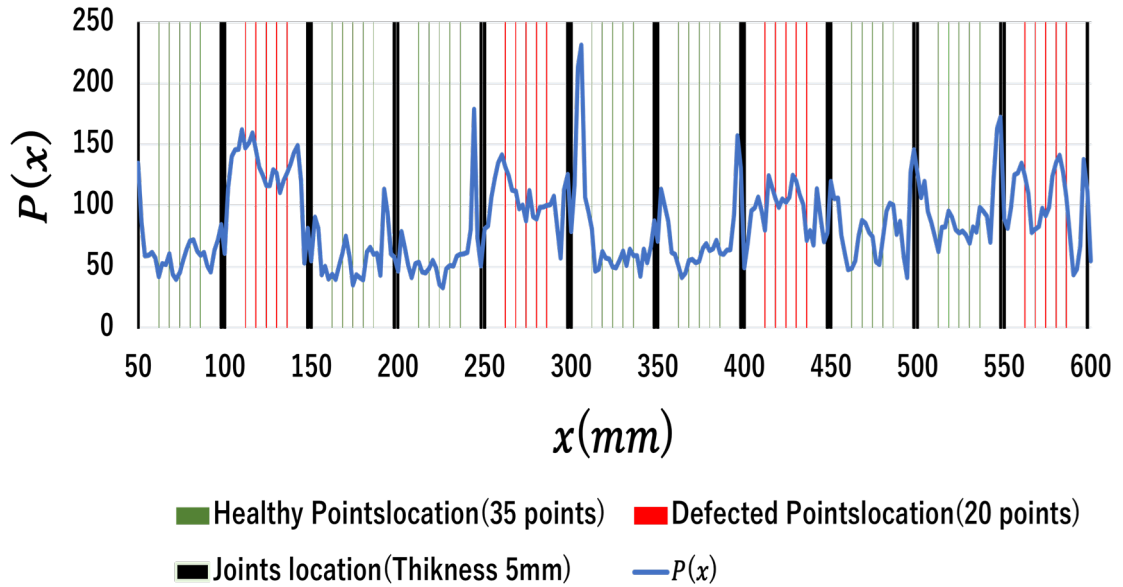
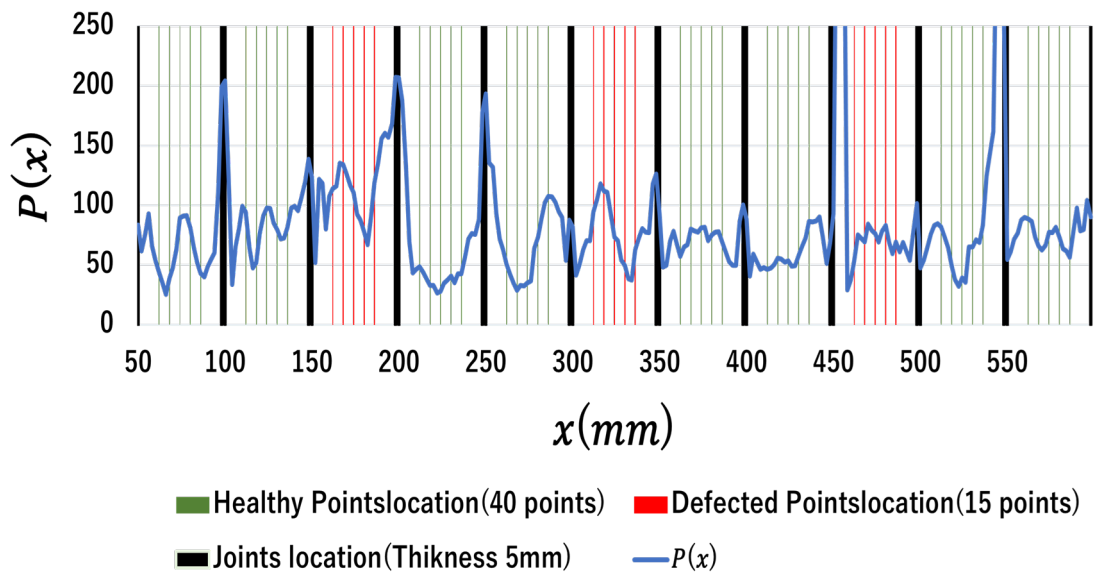(a) Distribution of Specimen1 B (2–12).
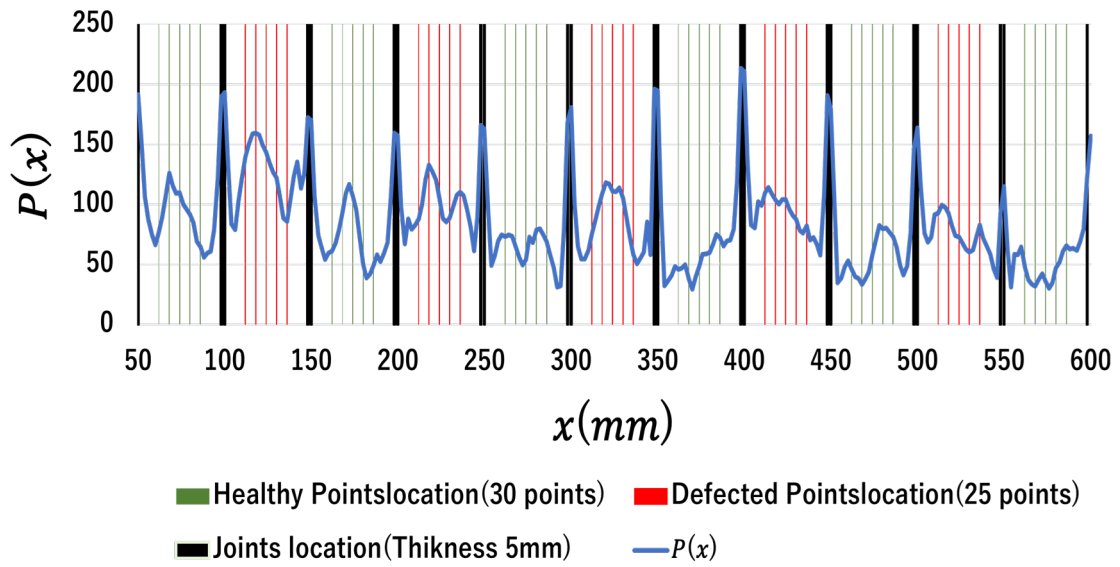
(b) Distribution of Specimen1 D (2–12)..

Figure 3.5: Measurement result

(c) Distribution of Specimen2 D (2–12)..

(d) Distribution of Specimen3 B (2–12)..

Figure 3.5: Measurement result

Table 3.3: Removing the tile.

| Tile Position	Void Size (%)	load (KN)	Load (N/m m2)	Reflection intensity integrated value range
Line D 425 /No.3	100	0.2	0.047	1995.184 ≦ V ≦ 2091.218
Line D 415 /No.3	100	0.2	0.047	2213.133 ≦ V ≦ 2748.449
Line B 225/No.3	100	0.2	0.047	2072.589 ≦ V ≦ 2542.316
Line B 215/No.3	100	0.2	0.047	1962.375 ≦ V ≦ 2526.109
Line D 425 /No.5	90	0.2	0.047	1883.54 ≦ V ≦ 2011.975
Line D 415 /No.5	90	0.2	0.047	2213.133 ≦ V ≦ 2748.449
Line B 225/No.5	90	0.5	0.12	978.187 ≦ V ≦ 1255.611
Line B 215/No.5	90	0.5	0.12	1962.375 ≦ V ≦ 2526.109
Line D 425 /No.7	70	1.8	0.42	1080.095 ≦ V ≦ 1262.066
Line D 415 /No.7	70	1.8	0.42	1611.007 ≦ V ≦ 2260.261
Line B 225/No.7	70	2.5	0.58	1155.665 ≦ V ≦ 1364.436
Line B 215/No.7	70	2.5	0.58	1310.026 ≦ V ≦ 1448.278
Line D 425 /No.9	50	2.3	0.54	1403.196 ≦ V ≦ 1577.651
Line D 415 /No.9	50	2.3	0.54	1727.914 ≦ V ≦ 2026.609
Line B 225/No.9	50	1.5	0.35	1532.733 ≦ V ≦ 1744.206
Line B 215/No.9	50	1.5	0.35	1402.269 ≦ V ≦ 1674.877
Line D 425/No.11	30	1.8	0.42	1244.876 ≦ V ≦ 1533.132
Line D 415/No.11	30	1.8	0.42	1403.842 ≦ V ≦ 1755.788
Line B 225/No.11	30	4.5	1.05	379.77 ≦ V ≦ 739.217
Line B 215/No.11	30	4.5	1.05	964.475 ≦ V ≦ 1316.536
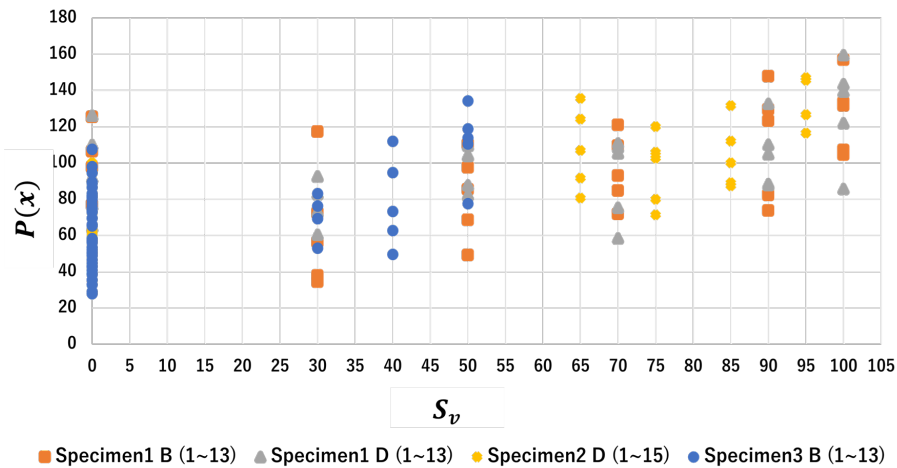
Figure 3.6: Result for the void size and results obtained with MLS

Table.3.3 row 2 and 3.

### 3.6.3   Adhesive strength measurements and MLS result data

Fig.3.12 shows the locations of each tile and its tested adhesion strength. Six points of the adhesion strength were placed at a total distance of $20mm$ and $\pm 10mm$ from the joints to avoid joint effects. The adhesive strength was measured at these six points. The recorded data of the tile peeling test and MLS is shown in Table 1. Row 1 shows the location of each tile whose adhesion strength was tested and scanned by MLS. Row 2 is the size of the void from 100% to30%, at a difference of 20%. Row 3 shows recorded data in Kilonewton (KN), which is the power consumed to remove the tiles. it appears directly in the analog load cell. In row 4 the power is converted to Newton per square millimeters (N/mm2). The MLS result data is shown in row 5. Based on Fig.3.12, Fig.3.3, and Fig.3.13, a scattergram plot created. It shows all the lines of the adhesive strength on the horizontal axis and the integrated value of the reflection intensity on the vertical axis. The intersection of the two values is shown by color. The gray points are Line B 215, blue points are Line B 225, yellow points are Line D 415, and orange points are Line D 425. This distribution suggests that there is a negative correlation between the two values.

3.6.4   Adhesive strength measuring and MLS result's data analysis

The adhesive strength data and MLS scattergram plot Fig.3.13, indicated that there is a negative correlation between the adhesive strength and the adhesion strength. Moreover, there appears to be a linear relationship between the two variables. The correlation coefficient result reveals that the two values have a strong negative correlation: decreasing the adhesion strength is correlated with increases in the integrated value of the reflection intensity $R = -0.622, p < .001,$. Furthermore, regression analysis was conducted. The R-squared and p-value were $R^2 = 0.382, p < .001$. Table.3.3 reveals that Line D 425 of tile No 3 has a void size bigger than that of tile No 5. Therefore, it should have a higher value of $P(x)$. However, the integrated value of the reflection intensity difference is low. Moreover, Line B No7 and No 8 have the same issue. These issues might be due to the uncured setup of the sheet. The environmental effects on sheet strength due to the time duration between the MLS scanning and adhesion strength measurement test should be taken into
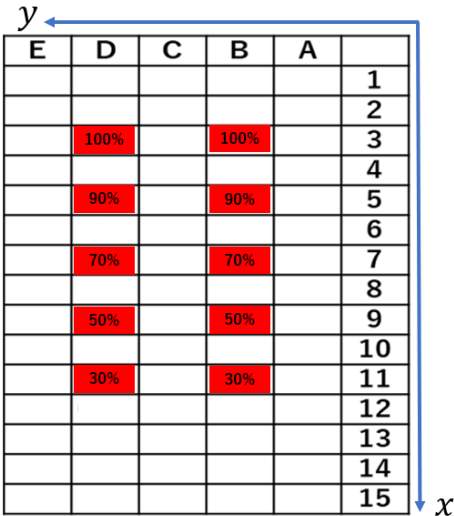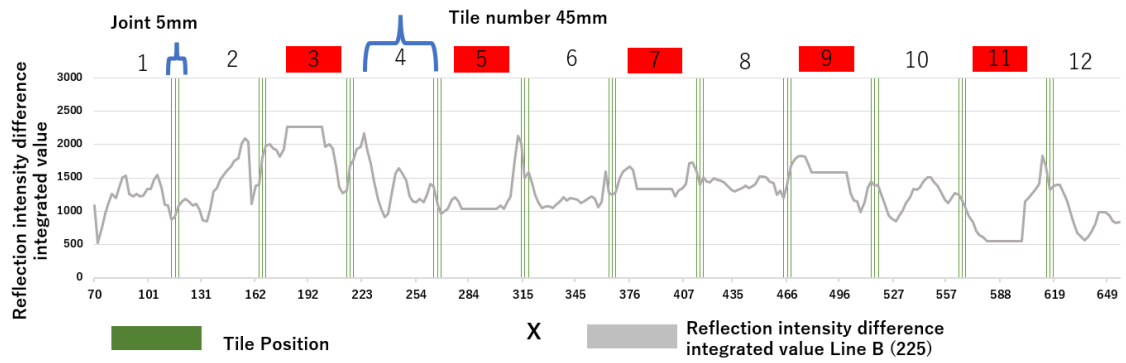
(a) Void distribution of Specimen1 A and
B.
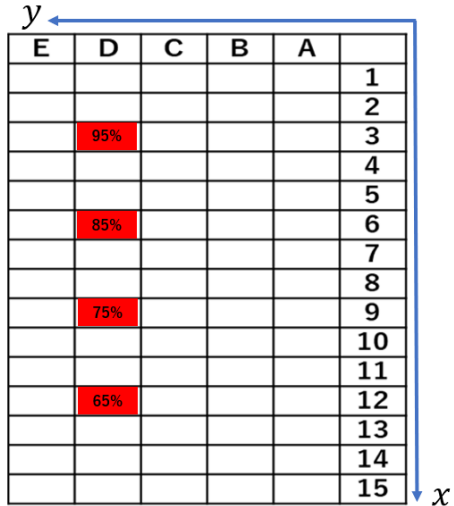
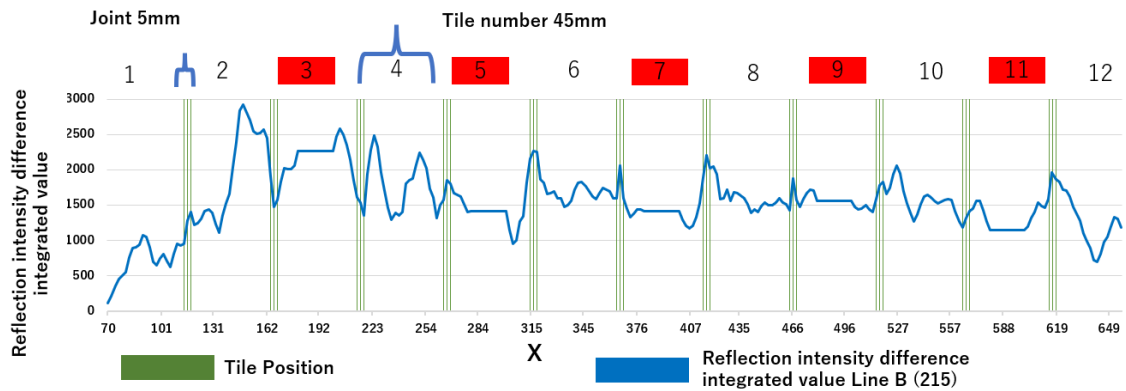(b) Void distribution of Specimen1 D
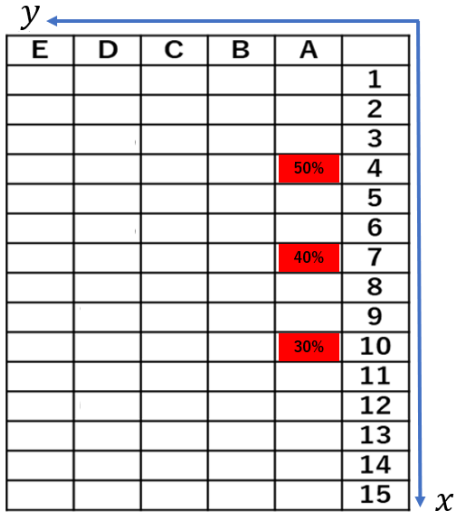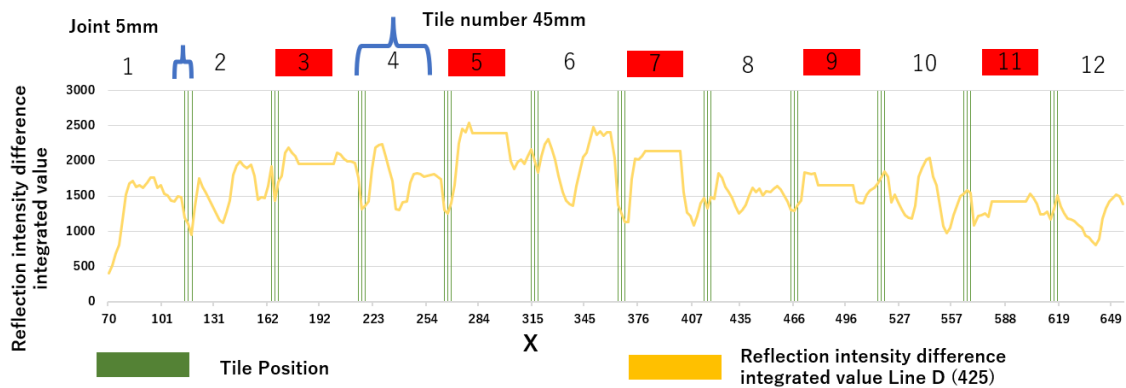
(c) Void distribution of Specimen2 D

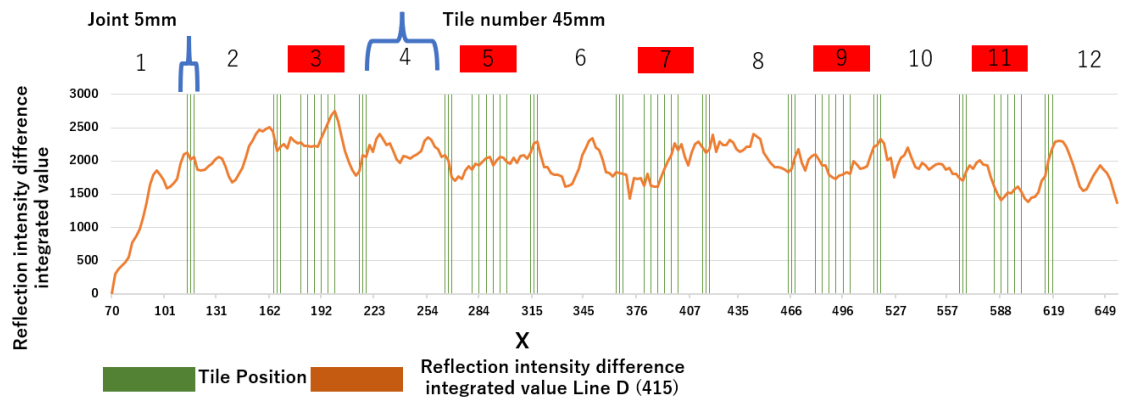Figure 3.7: Void location on specimen

(a) Distribution at Y=215mm (Line B 225).

(b) Distribution at Y=225mm (Line B 215).

(c) Distribution at Y=415mm (Line D 425).

(d) Distribution at Y=425mm (Line D 415).
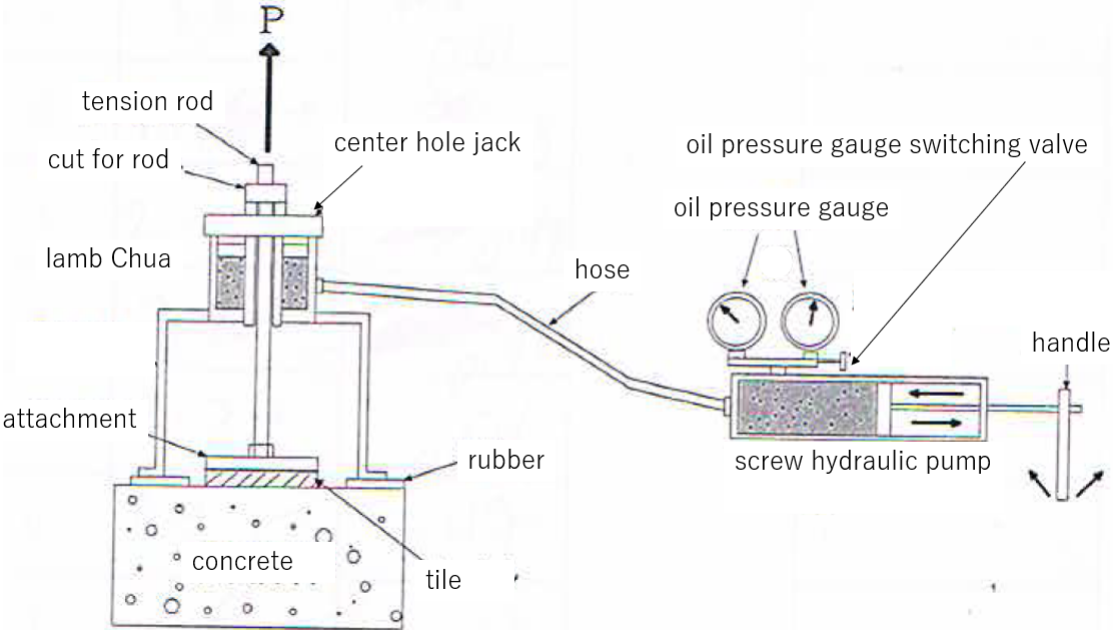
Figure 3.8: Distribution of $P(x)$

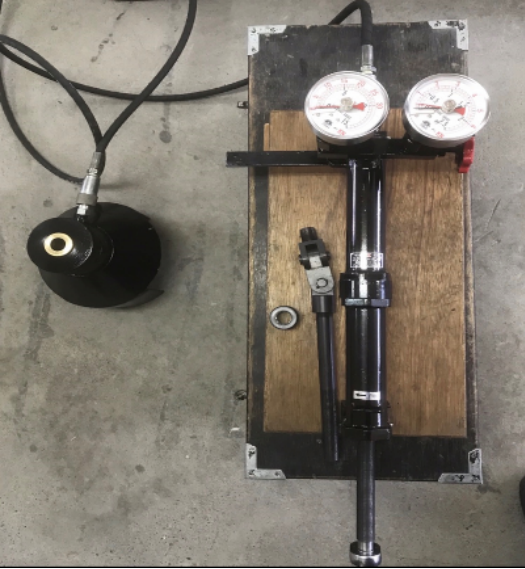Figure 3.9: Components of the research type adhesion tester.

Figure 3.10: Research type adhesion tester.

Figure 3.11: Removing the tile.

consideration. To improve the accuracy of the estimation, it is important to implement this method using more tiles of different sizes to have more data to analyze. In addition, the experimental procedure must be improved to obtain the MLS scanning data and the adhesive strength at the same time. Furthermore, a more accurate adhesive strength measurement device should be used.

3.6.5 Discussion

The results revealed that the adhesion strength can be estimated, but the error between the actual and estimated values is still large. The regression analysis of R is significantly low. This low value might be due to the experiment procedure or the unsuitability of the sheet that was implanted under the tile. In Fig.3.12a Line D 425 tile No.3 has a void size bigger than that of No.5. Therefore, it should have a higher value of $P(x)$. However, the integrated value of the reflection intensity difference is low. Furthermore, Line B No.7 and No.8 have the same issue. These issues might be due to the uncured setup of the sheet. The environmental effects on sheet strength due to the time duration between MLS scanning and adhesion strength measurement test should be taken into consideration. To improve the accuracy of estimation, it is important to implement this method using more tiles of different sizes to have more data to analyze. Moreover, the experiment procedure must be improved to obtain the MLS scanning data and the adhesive strength at the same time. Furthermore, a more accurate adhesive strength measurement device should be used.

3.7 Disadvantages of MLS and the basis of optimization

MLS theory is based on changing the dm at the same point. However, ensuring that the device maintaining an exact position is technically tricky and increases inspection time and cost. Furthermore, the quality of data obtained in cases where the scans are conducted at an inappropriate height makes the application of this technology far from practical. Therefore, scanning time should be reduced to make MLS more efficient, and reasonable results should be guaranteed.
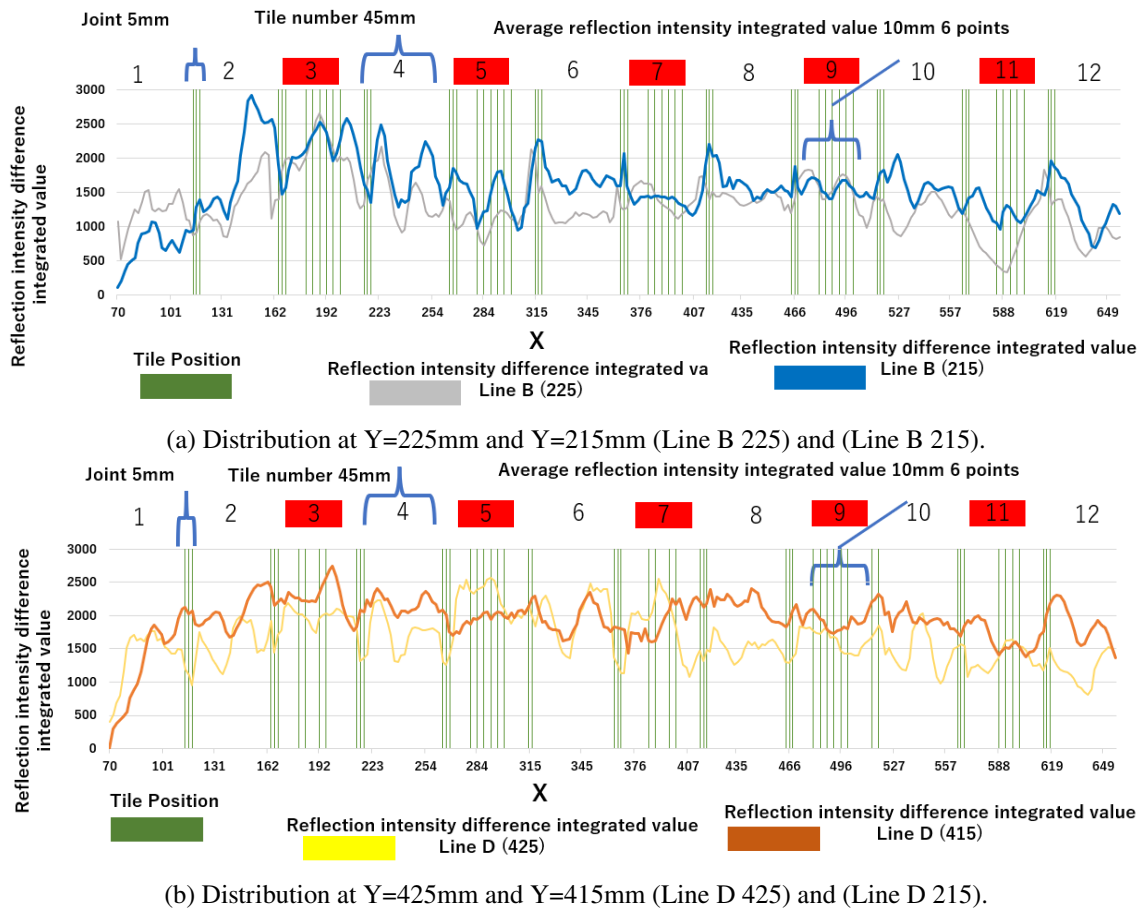
(a) Distribution at Y=225mm and Y=215mm (Line B 225) and (Line B 215).

(b) Distribution at Y=425mm and Y=415mm (Line D 425) and (Line D 215).

Figure 3.12: Adhesion strength points distribution

3.7.1   Simulation method and conditions

A simulation was conducted to determine the appropriate layers to calculate the value of ΔE, and 3.14 shows the simulation scenario. First, several layers of healthy tiles were surveyed, and the E_T value was measured. Fitting was performed using the mathematical model of Eq.2.13 to calculate $\hat{E}_T(E_T$ calculated by the model). Scanning was also performed for several layers on different defective tiles with different S_v sizes to measure the value of $\hat{E}_V(E_v$ calculated by the model)using the mathematical model of Eq.2.21. Subsequently, fitting was performed using the mathematical model of Eq.2.21 to calculate $\hat{E}_T$. Then, ΔE and $\Delta \hat{E}$ values were extracted and their linear relationship was compared with the S_v sizes. Finally, the linear relationships of ΔE and $\Delta \hat{E}$ with S_v were compared. If the S_v values are identical, then the appropriate layers can be determined through simulations only if the d_v values are already known. The scenario of the simulation as follows:

- E_T value was measured. Fitting was performed using the mathematical model of E_T to calculate $\hat{E}_T$

- E_v value was measured. Fitting was performed using the mathematical model of E_v to calculate $\hat{E}_v$
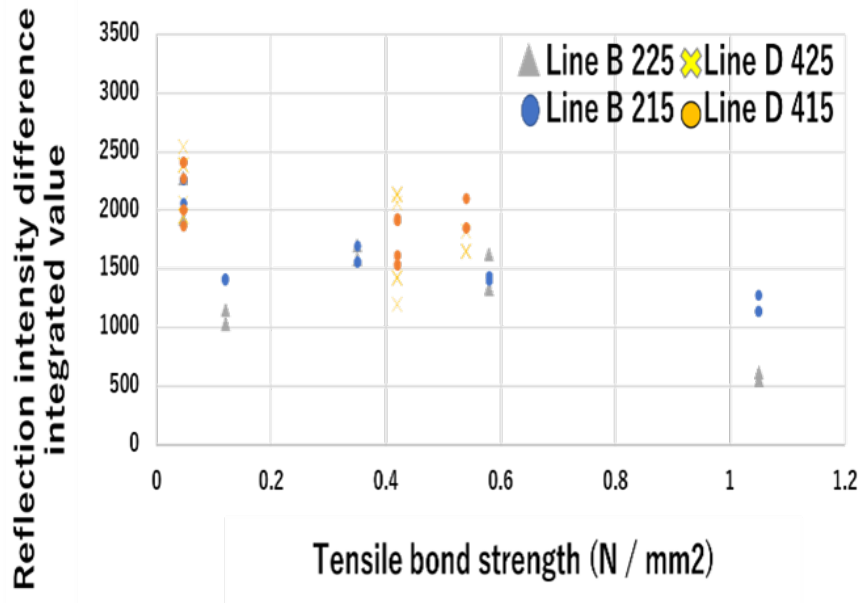
- ΔE an $\Delta \hat{E}$ value were extarcted

Figure 3.13: Integrated value of the reflection intensity and adhesion strength graph.

- Compared the liner relationship of ΔE and $\Delta \hat{E}$

- Compare the result data of both measured and calculated data

3.7.2 MLS scan, result of ΔE and $\Delta \hat{E}$, and discussion

MLS was conducted on four samples of tiles containing voids of different sizes and six healthy tiles, as shown in Fig.3.15. Tiles no. 3 ($S_v = 100\%$), 5 ($S_v = 90\%$), 7 ($S_v = 70\%$), and 9 ($S_v = 50\%$) in line B are defective tiles, and tiles 2, 4, 6, 8, 10, and 11 are healthy tiles. The wave reflection intensity was obtained by scanning nine times along the x-axis in each scanning area at $64mm < d_m < 72mm$. Subsequently, a simulation of E_T was performed using3.16, followed by a simulation of E_v using 2.21. Simulations and comparisons were performed in the same sequence as shown in 3.15. The results were divided into two parts based on correlation and slope: one with a high correlation of $\Delta E > 0.60$ and high slope of $\Delta E > 0.40$. The same conditions were applied to $\Delta \hat{E}$. The data were measured. 3.18a depicts the relationship between ΔE and S_v with a high correlation and slope. 3.18b shows the measured data with a low correlation and slope. 3.18c depicts the relationship between$\Delta \hat{E}$ and S_v with a high correlation and slope. 3.18d shows the calculation results of data with a low correlation and slope. In addition, Fig.3.18a shows the plots of the slope and correlation of measured data, and 3.18a shows the plots of the slope and correlation of simulated data. All the results are listed in Table 1. The slope in3.18 proves that the linear relationship of ΔE and $\Delta \hat{E}$ with S_v on each layer correlates with $R = 0.92$

In the case of the defective tile, E_v was measured (Fig.3.17) . Fitting was performed using the mathematical model of E_v 2.21. For fitting the least squares method, the parameters α, d_v were adjusted.

In this section, an optimization was performed for the scanning layers of voids using electromagnetic waves via MLS. Furthermore, an actual scan conducted on concrete tiles containing several voids
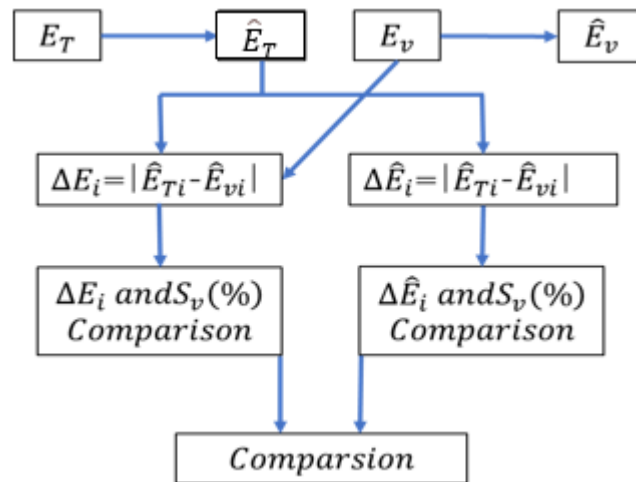
Figure 3.14: Flow of the simulation and comparison between ΔE and $\Delta \hat{E}$
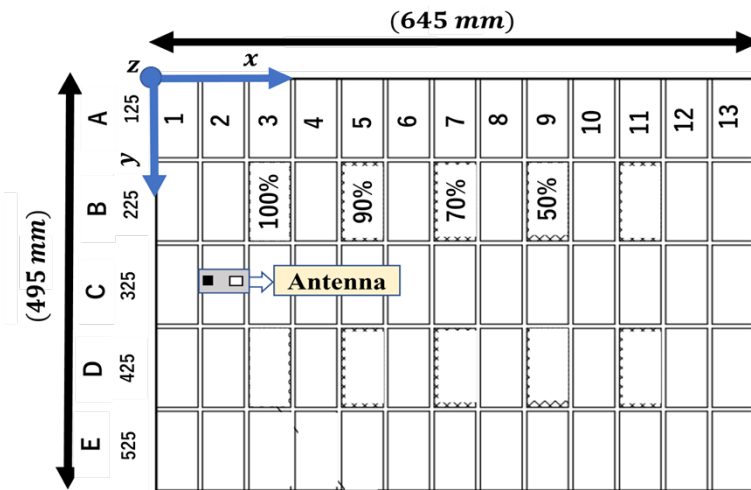

Figure 3.15: Overview of the healthy and defective tiles

showed different plane sizes. The experimental results were compared with the simulation results for each layer and were in good agreement. As shown in Fig. 3.19a and Fig. 3.19b, when scanning using layers at $d_m = 65, 66, 67,$ and $68mm$ for both the measured and simulated data, it was possible to obtain ΔE However, when scanning using layers at $d_m = 64, 70, 71$ and $72mm$, it was not possible to obtain the correct data for ΔE. By scanning the layer at $d_m = 67mm$, the best data for ΔE was obtained. In addition, it was possible to obtain good quality data by scanning only once (single-layer scan). One-time scanning is a valuable advantage of this method because scanning the same point multiple times is difficult. In addition, considering that scanning multiple times is time-consuming, it is essential to optimize the number of scanning layers. Thus, according to the results, it is possible to find the size and location of the void by scanning once but with the condition that the value of d_v is known. However, the effect of the change in void depth on ΔE could be observed using simulations based on the mathematical model given in Eq.2.16 for E_T and in Eq.2.16 for E_v.
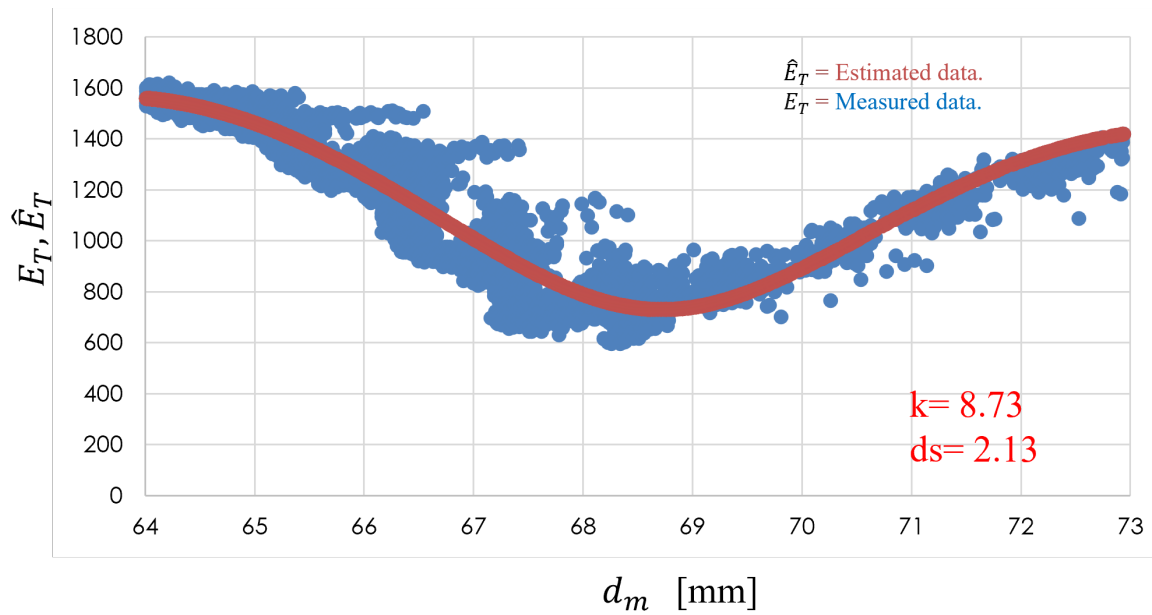
Figure 3.16: Fitting of healthy tile data using the E_T mathematical model

3.8 Conclusion

In this chapter, The effectiveness and necessity of the MLS methodology for measuring voids without requiring the void depth, d_v, is confirmed. Next, a methodology for extracting the void information is presented. Accordingly, an actual tiled specimen with various void plane sizes was scanned using an inspection device. Finally, the results of the experiment revealed the ability of the proposed method to determine the void information, and the correlation between the void depth and the void plane size was $R = 64$. we explained to detect voids in tiles, the scanning layer was optimized for non-destructive inspection using electromagnetic waves and MLS technology. First, the mathematical models of Eq.2.16 for E_T and in Eq.2.16 for E_v were explained. Then, the procedure for comparing the measured and simulated data developed, as shown in Fig.3.14. Subsequently, the MLS scanning experiment was conducted on several tiles containing several voids of different plane sizes. The results were compared, as shown in Fig.3.19a and Fig. 3.19b. Finally, the experimental and simulation results showed a correlation of $R = 0.92$ in the slope case. The relation between reflected waves of defective tiles and adhesion strength and tile was proved. First the MLS conducted to obtain the P(x) value of the voids under tile. The P(x) value is changing along with the void size. After that same tile that included voids has been removed using bonding tester. The maximum force that required to remove the tile was recorded. Finally, the P(x) value and the bond strength had negative correlation, which is decreasing the power of adhesion strength were correlated with increases the Reflection intensity integrated value R= -0.62.
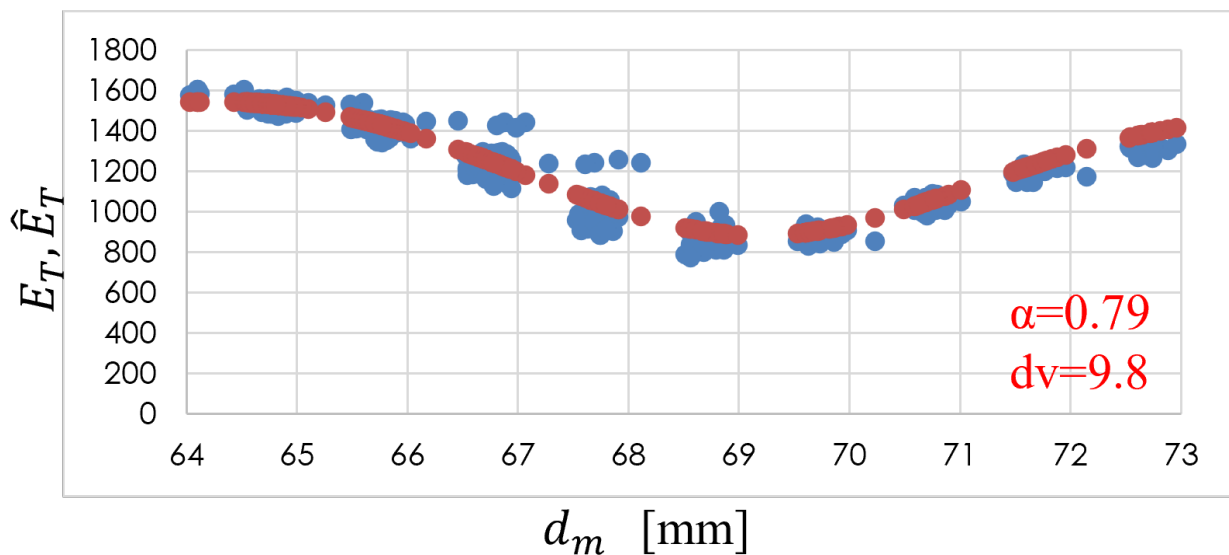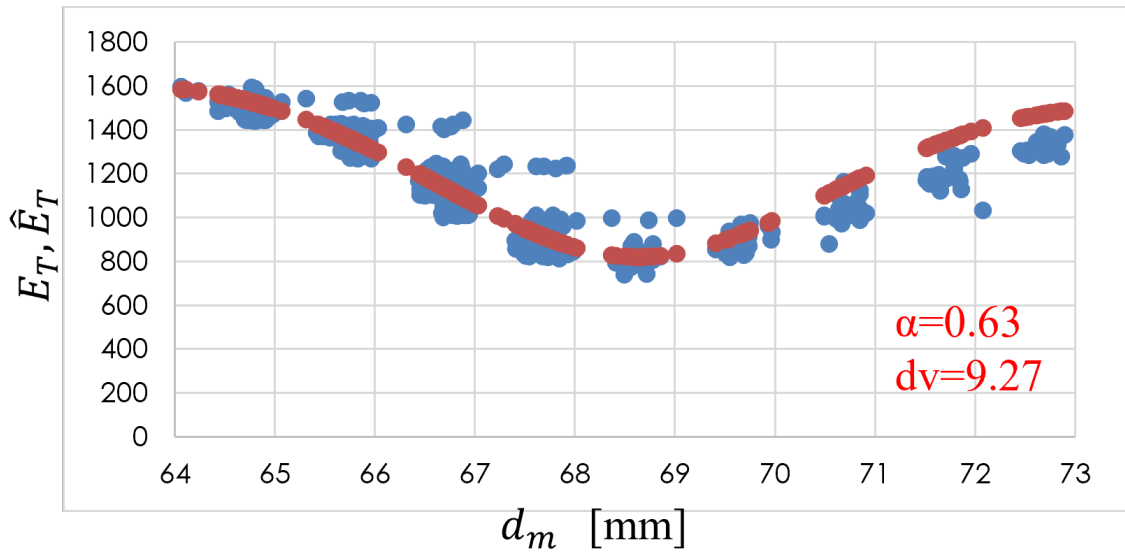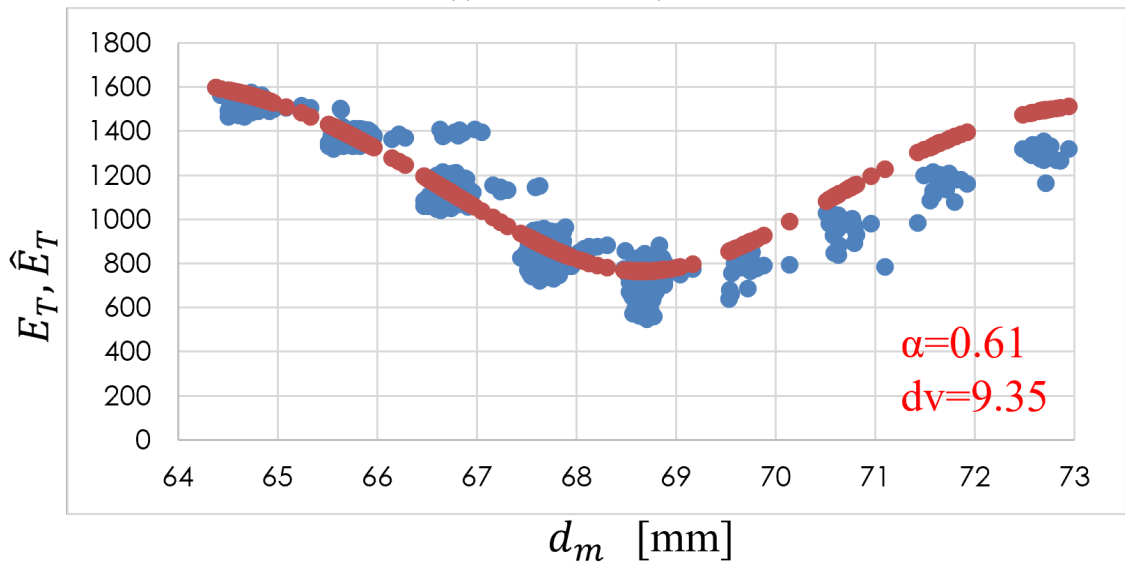
(a) Void size = 100%).
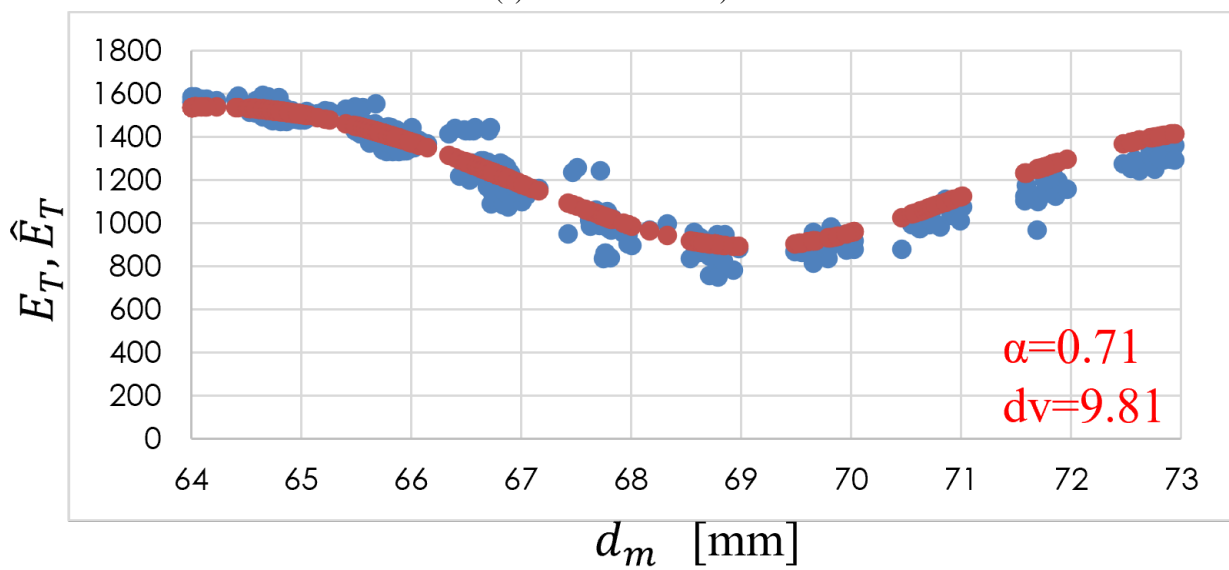
(b) Void size = 90%.
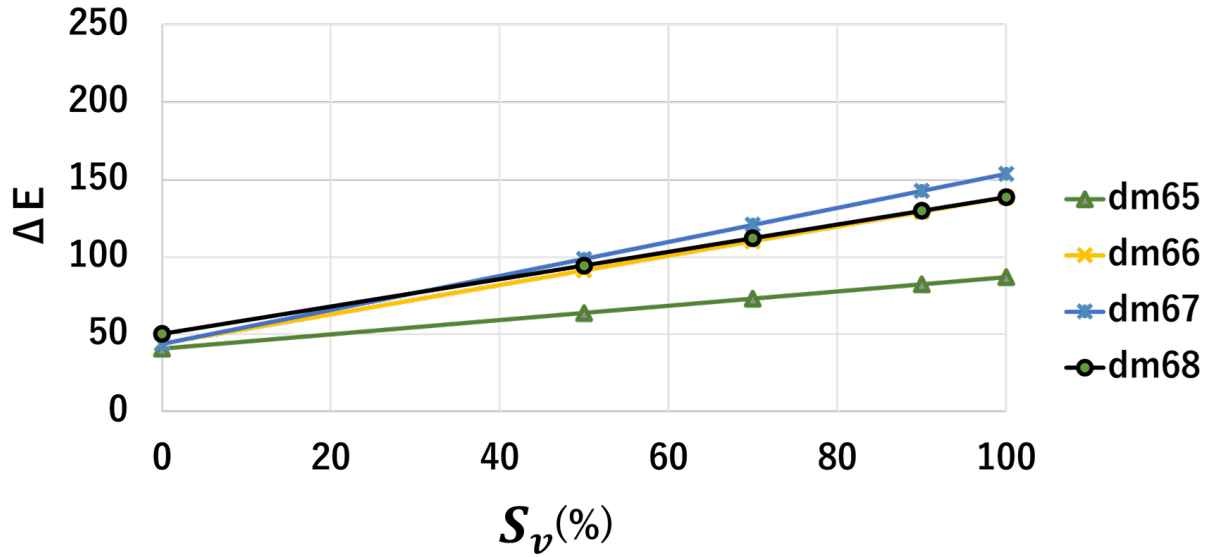
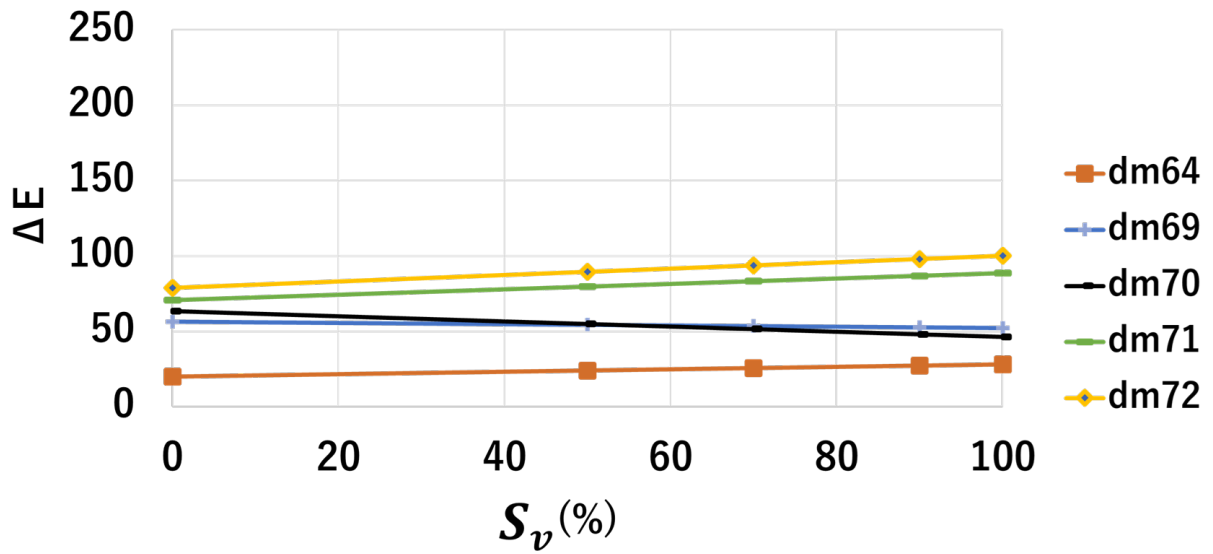Figure 3.17: Measured data of the defective voids

(c) Void size = 70%).

(d) Void size = 50%.
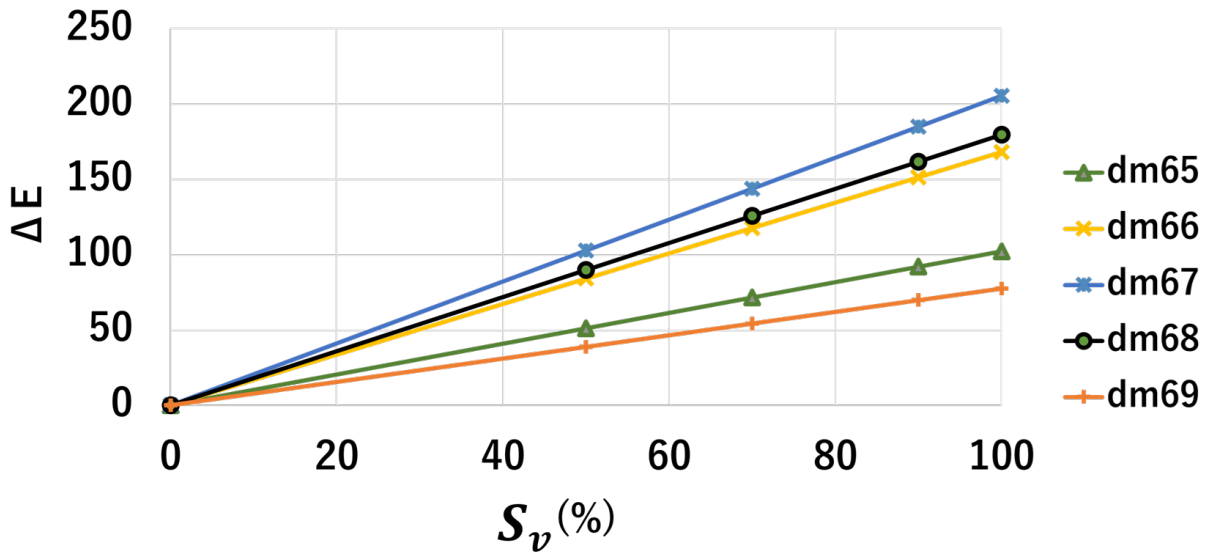
Figure 3.17: Measured data of the defective voids

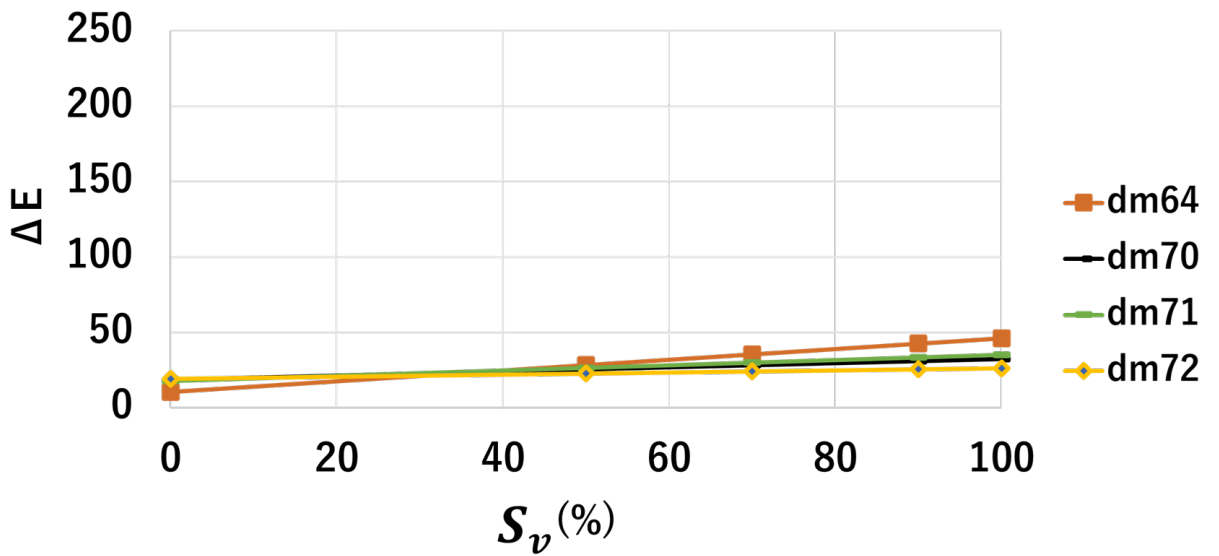(a) $DeltaE$ and S_v high correlation and slope.

(b) ΔE and S_v low correlation and slope.

Figure 3.18: Comparing ΔE and $\Delta \hat{E}$ with S_v in each d_m
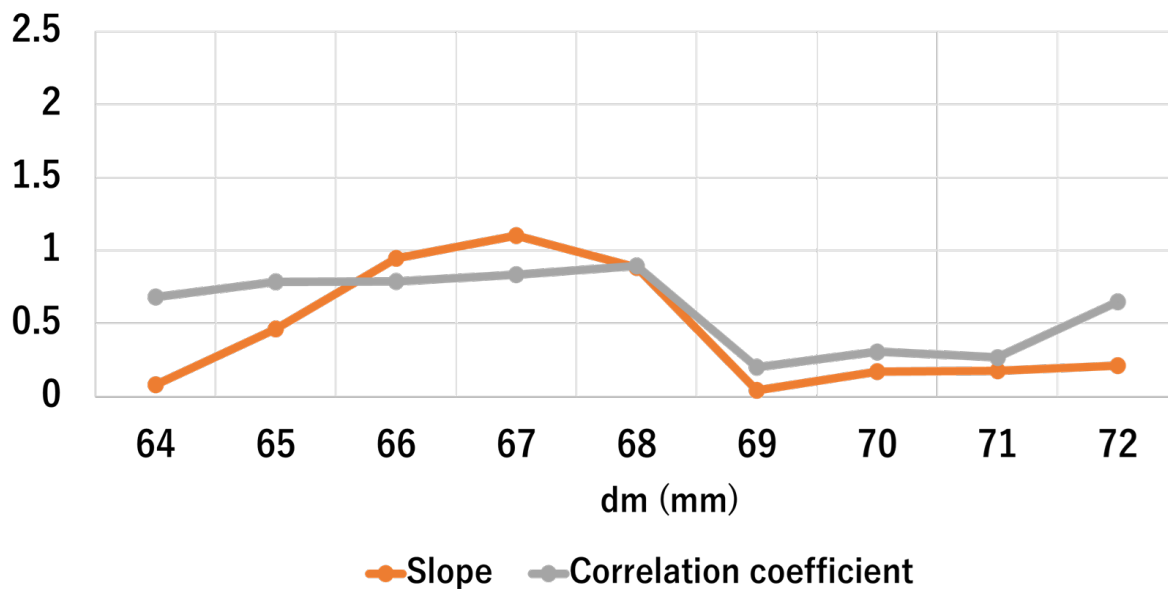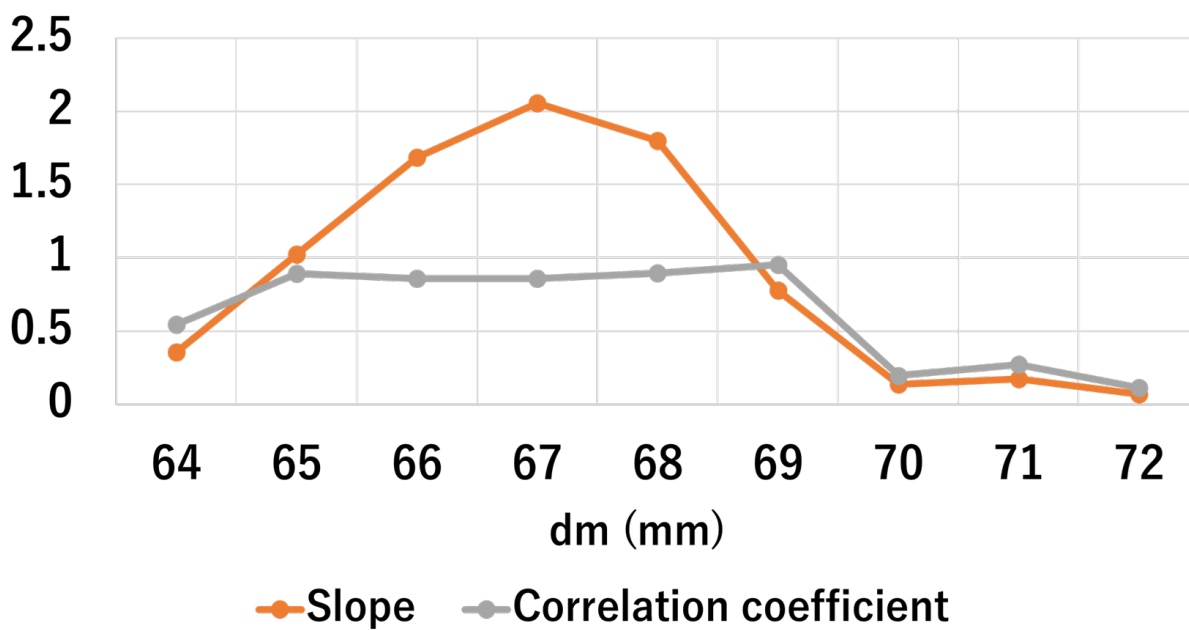
(c) $\Delta\hat{E}$ and S_v high correlation and slope.

(d) $\Delta\hat{E}$ and S_v low correlation and slope.

.

Figure 3.18: Measured data of THE defective voids

(a) Correlation and slope of ΔE

(b) Correlation and slope of $\Delta \hat{E}$

Figure 3.19: ΔE and $\Delta \hat{E}$ correlation and slope

Chapter 4

Estimation of the void depth and reflectance

4.1 Vertical scanning method

Multiple scans have been made on healthy and defective tile. The scanning method in this section is different from that in the previous chapter. The method involves fixing the antenna portion directly above the tiles so that the X and Y axis of the actuator are fixed, and the only moving one is Z. When Z moves vertically, the d_m change, so we can obtain E_T or E_v for different d_m. This method gives more accurate data. In previous methods, the antenna was passed over the same point at each d_m change. However, when the antenna is fixed, obtaining E_T or E_v data is better guaranteed. Fig.4.1 shows the vertical scanning method. The same antenna and actuator were used in the experiment. The frequency was 10 GHz as shown in Table.2.9. Therefore, the wave length was 30 mm. To ensure the restoration of a sine wave, more than 1/4 of the wavelength should be measured.

4.2 Theory of estimating void depth and plane size

The mathematical model of the reflected waves from the healthy tiles E_T in Eq2.18is based on calculating the l_s in Eq.2.8 and k. The method of calculating the l_s and k optimizes the parameters using the least square method as shown in Eq.3.3. On other hand, the two parameters l_v and k need to be optimized for waves reflected from voids. However, as we use the same tiles, k of both E_T and E_v have the same value. In addition, the strength of the waves reflected from the void is effected by the void plane size(Eq2.24). The void size effect is considered in Eq2.21. Finally, the two parameters l_v and α can be estimated using least squares method. In Eq. 2.21, the value of E_5 and α has effect to E_v. In the case of $\alpha = 0$, the value of E_v will be same as that of E_T, which indicates that there is no void. In addition, when the void size is small, the value of α will be small, which will indicate that the value of E_v is close to value of E_T.

4.3 Methodology of estimation of both void depth and reflectance

Chapter2 explain the model of calculating the $\hat{E}_T(E_T$ using Eq.2.13 and the model used to calculate the $\hat{E}_v(E_v$ using Eq.2.21. Theoretically, we notice that, in these models, the value of α indicates the plane size of the void. Moreover, the value of d_v indicates the depth of the void. A practical
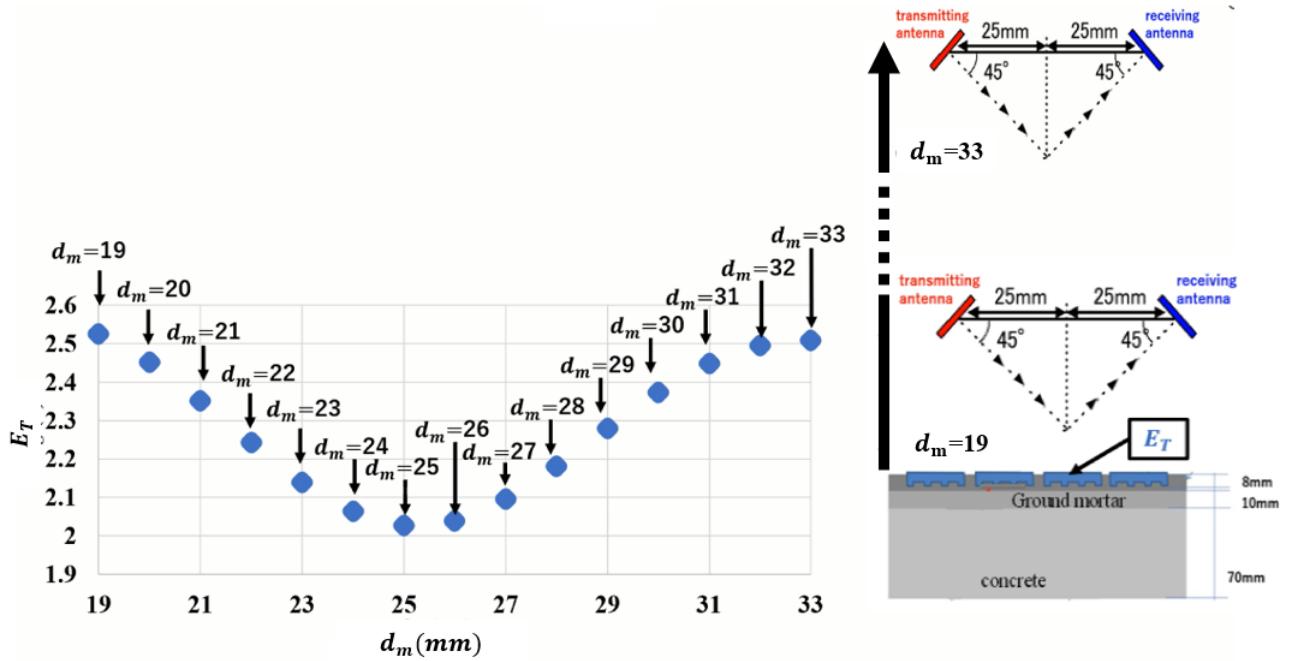
Figure 4.1: Value of E_T for each d_m

experiment was carried out on real tiles that contain defective tiles with different sizes and depths. Then, the steps shown in Fig. 4.2 were taken. First, the healthy tiles were measured to obtain the value of E_T, and then calibration was done using Eq. 3.3, where the variables are k (reflection coefficient) and d_s (Synthetic Waveform). After that, the defective tiles were determined, and the calibration was done using Eq.4.1, where the variables are alpha (Reflectivity) and devi(void depth). It should be noted that the value of k is the same as that used in the calibration of healthy tiles.

$$\min_{\alpha,d_v} \sum_{i=1}^{N} (\hat{E}_v(x, d_m j) - E_v(x, d_m j))^2 \tag{4.1}$$

4.4　Experimental result and discussion

The experiment conducted on real tiles included defective tiles with different size and depth (Fig. 4.3).First, an MLS scan conducted on both healthy and defective tiles. The calibration was then performed using the measured E_T. This calibration was the same one used with measured E_v. Finally, the measured and estimated void depths and void plane sizes were compared. The values are listed in Table1.1. Fig.4.4 shows the relation between the estimated and measured voids depth, with a R=0.86. Similarly, Fig.4.5 also shows the relation between the measured and estimated void plane size, with a correlation of R=0.91.

It has been proven that the plane size and depth of the void can be predicted. However, in this study, the void shape is equal to the shape of the tiles and has a regular geometric shape. However, it is possible to predict the depth and plane size of a void that has a regular geometric shape that is

1. Value of E_T was measured.
2. Calibration was performed using the mathematical model of E_T
3. Calculate k and d_s
4. Value E_v was measured.
5. Calibration was performed using the mathematical model of E_v
6. Calculate α and d_v
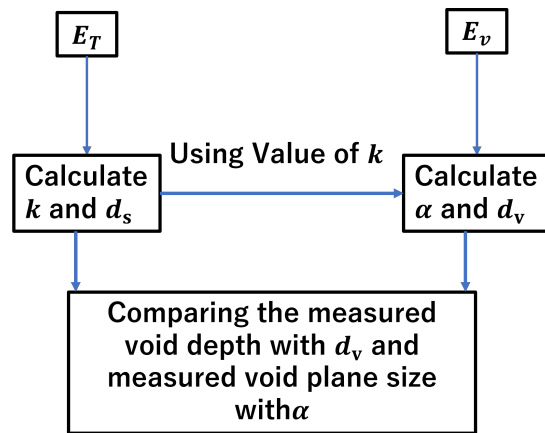7. Comparing the measured void depth with d_v and measured void plane size with α

Figure 4.2: Void depth and plane size value extraction chart

different from the shape of the void or that has an irregular geometric shape because the voids in tiles are often of irregular geometric shape. Furthermore, only one void was made under the tiles in this study; thus, the results herein might not be applicable to situations in which there are more voids under a tile.

4.5   Conclusion

In this chapter, a method for predicting the plane size and depth of the void is explained, based on the mathematical model of E_T and E_v through optimization of l_s and k for healthy tiles and l_v and α for defective tiles. An experiment was then conducted on tiles that contained voids of different plane sizes and depths. The void sheet has the same representation and measurements shown in Fig.2.7. Then, a vertical scan was conducted on both healthy in defective tile. Then, we optimized l_s and k for E_T and d_v and α for E_v. Finally, the calculated value of d_v was compared with the value that was measured. The results of the comparison revealed that it has a relationship equal to R = 0.97 as shown in Fig.4.4. Furthermore, the value of α has a relationship with the value of the measured void plane size, with R = 0.91 as shown in Fig.4.5.

Table 4.1: Measured and estimated void depths and void plane sizes

Tile Number 0	Measured void depth	d_v Estimated Void depth	Measured void size	α Estimated void size
E8	20mm	18.33	1	0.973
D8	24mm	23.46	1	0.835
C8	28mm	28.60	1	0.892
B8	32mm	33.54	1	0.854
A8	35mm	33.76	1	0.990
E14	20mm	18.28	0.8	0.813
D13	24mm	23.78	0.8	0.806
C14	28mm	28.70	0.8	0.831
B14	32mm	33.62	0.8	0.700
A14	35mm	33.75	0.8	0.999
D4	20mm	23.57	0.4	0.64
D3	20mm	18.52	1	0.75
D6	20mm	18.49	0.7	0.74
D9	20mm	18.39	0.5	0.73
D12	20mm	18.47	0.3	0.62
A15	1.73	0.08	0	0.08
B15	3.46	0.19	0	0.19
C15	5.35	0.33	0	0.33
D15	8.89	0.39	0	0.39
E15	7.67	0.01	0	0.01
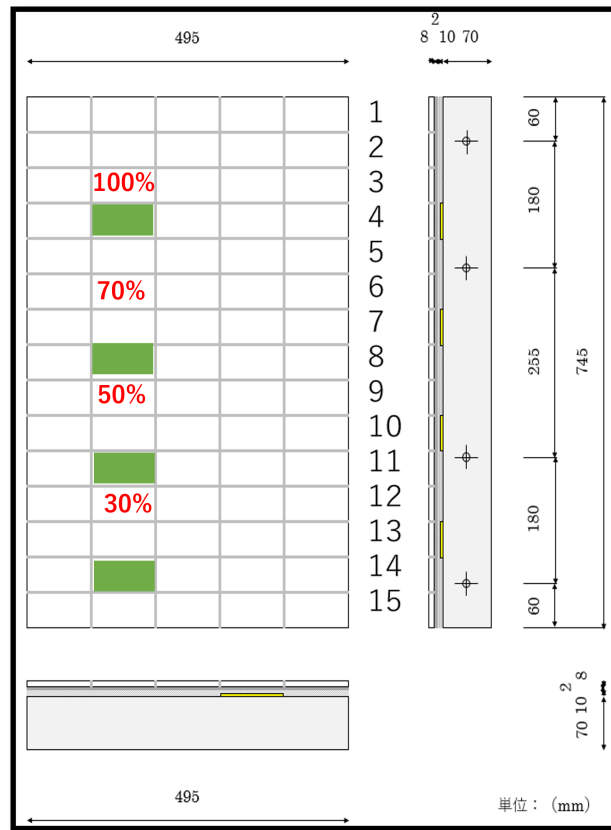
(a) Distribution of the voids and healthy tiles of specimen1
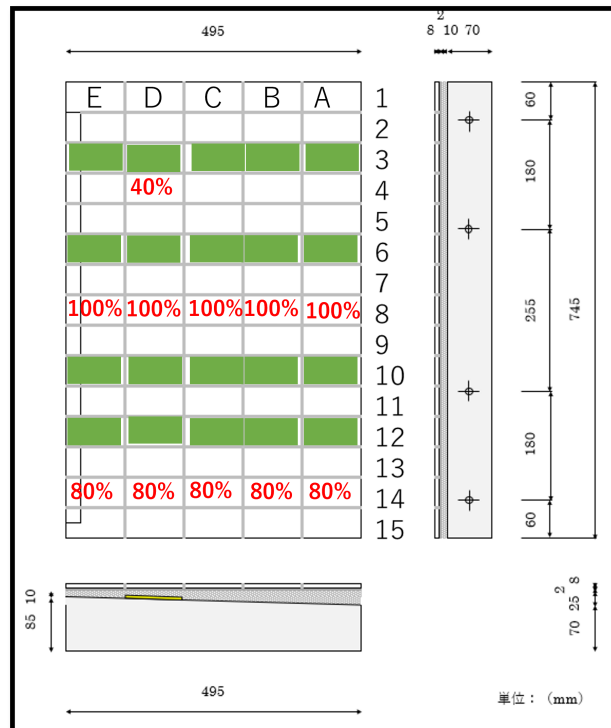
(b) Distribution of the voids and healthy tiles of specimen2

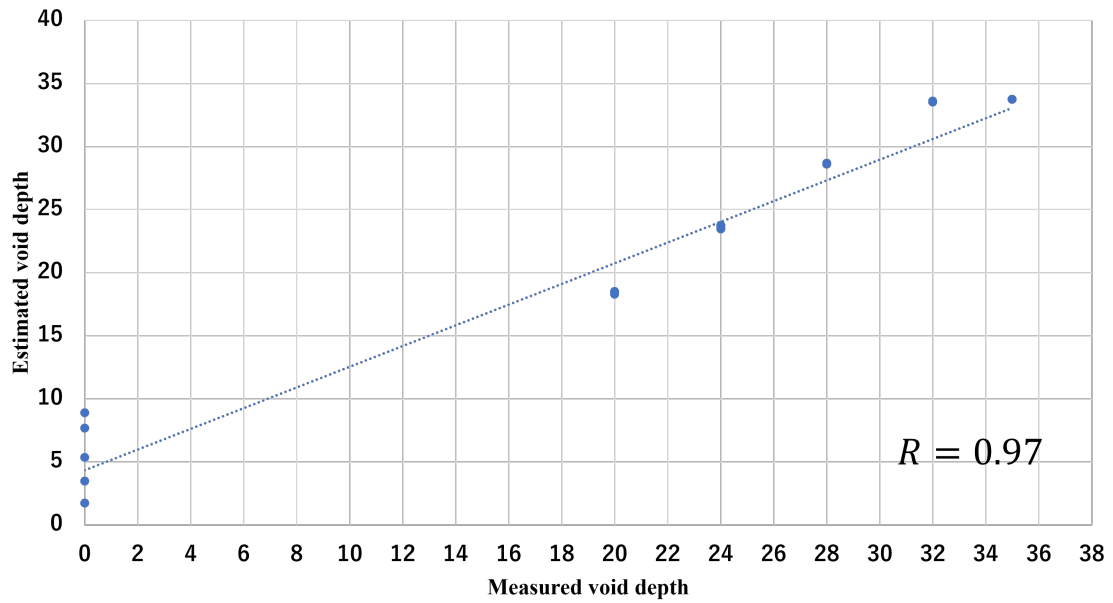Figure 4.3: Location of voides on the specimen

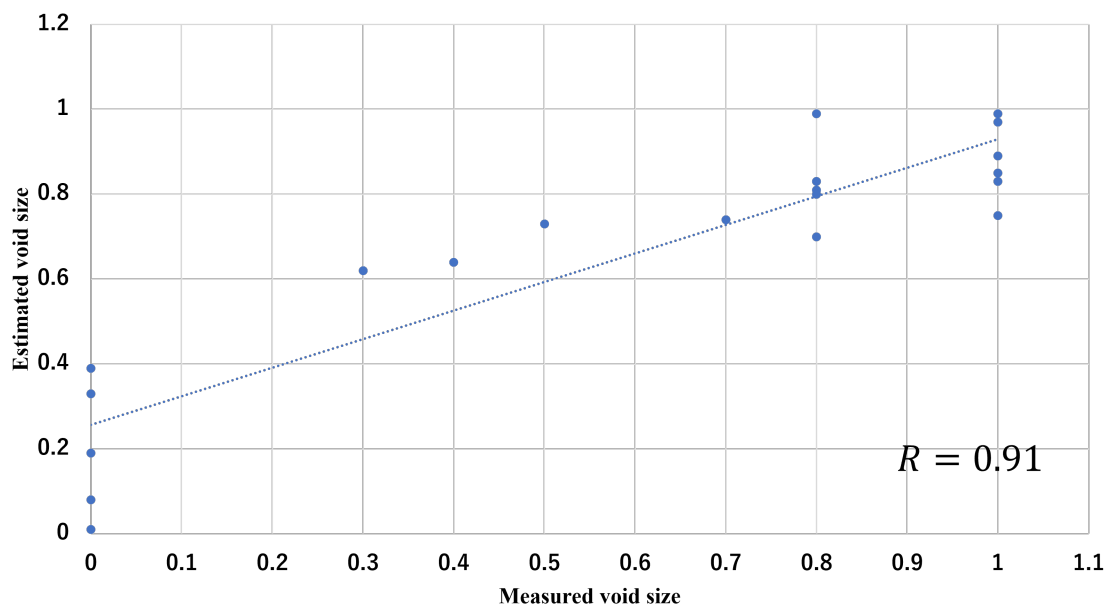Figure 4.4: Relation between the estimated and measured void depths

Figure 4.5: Correlation relation of the measured and estimated void sizes

Chapter 5

Conclusions and future studies

5.1 Conclusion

First, this study proposed a methodology for detecting voids under outer wall tiles using electromagnetic waves. The methodology's efficiency and ability were proven via experiments. Experiments were conducted using a micro-strip antenna and MLS on actual connected concrete wall tile specimens. After studying The properties of wave reflection of electromagnetic radiation, the study developed a mathematical model of the reflection of defective and healthy tiles. These models allowed this study to go beyond detecting voids to detecting void sizes and optimizes the MLS. This study also proposed a method for estimating the adhesion strength of tiles by comparing the void's size and the peeling strength of tiles. This study also focused on developing a method that allows non-experts to easily perform quantitative tests. Among the existing methods, by fixing the wavelength to be used for electromagnetic waves, it is possible to develop a compact, inexpensive device for measuring concrete voids that can be used by non-experts. In particular, the MLS method of the proposed method measures the "antenna probe", which has fixed transmitting and receiving antennae for microwaves, a type of electromagnetic wave, multiple times by changing the distance between the sample and the antenna. We have verified the possibility of creating a small and inexpensive air gap measurement device by utilizing scanning. The theory and mathematical model that is based on the idea of calculating the synthetic wave reflected from each layer in the case of healthy tile. In defective tiles, the model adds the value of the reflected wave from the void. The defective tile model also considers the effect of the void size on the total reflected waves. Therefore, the model can estimate the plane size and depth of the void.

Second, experiments were conducted on concrete specimens with attached objects (tiles) to verify the validity of the method. Section 2.2 describes the details of the concrete specimen used in this experiment and describes the details of the void sheet under the tiles. Furthermore, it also describes the details of the experimental method and measurement to confirms the validity of the proposed model.

Further, experiments were conducted on the same concrete specimens using MLS. The aim of the experiments was to ensure that the adhesion strength could be predicted by the strength of the waves reflected by the defected tile. First the MLS was conducted to obtain the $P(x)$ value of the voids under the tile. The $P(x)$ value varies with the void size. After that, the same tile that contained voids was removed using a bonding tester.The maximum force that was required to remove the tile was recorded. Finally, we found that the $P(x)$ value and the bond strength had a negative correlation, which was that decreases in the adhesion strength were correlated with increases in the reflection intensity integrated value. MLS is a technique in which a device's

height from the scanning point is changed at the same spot. It is time-consuming and technically challenging. Therefore, this study propose a method of optimizing the scanning of layers. First, the mathematical models of E_T and E_v were explained. Then, the procedure for comparing the measured and simulated data was developed. Subsequently, the MLS scanning experiment was conducted on several tiles containing several voids of different plane sizes.Finally, the experimental and simulation results showed a correlation of $R = 0.92$ in the slope case.

Finally, The method of predicting the plane size and depth of the void is explained, based on the mathematical model of E_T and E_v through optimization of l_s and k for healthy tiles and l_v and α for defective tiles. An experiment was then conducted on tiles that contain voids of different plane sizes and depths. The void sheet had the same representation and measurements. Furthermore, optimization of l_s and k for E_T and d_v and α for E_v were performed. Finally, the calculated value of d_v was compared with the value that was measured, the results of the comparison revealed that it has a relationship equal to R=0.97.Furthermore, the value of α has a relationship with the value of measured void plane size with R=0.9.

This study presented a unique method for detecting voids under tiles based on the strength of electromagnetic wave reflection from defective and healthy tiles. MLS method enabled the study to rely on the strength of reflection only, through the possibility of calculating the value of the void without prior knowledge of the value of the depth of the void. With the fixed frequency of the waves, the system becomes light in weight and low in cost. This study went beyond simply detecting the voids under tiles, it also focused on creating a mathematical model of reflectance. Mathematical models helped study the ability to optimize the scanning layers of MLS, which led to reduced scanning time and increase the efficiency of scanning data. Mathematical modelling also helped the study to find the relationship between adhesion strength and P(x). The study consisted of finding a connection between P(x) and the size of the void. Therefore, the study went to the development of mathematical models to predict both depth and size of the void. The study will open a new horizon in the world of non-destructive examination. Through the ease and inexpensiveness of the system developed in this study, we will expect the following:
1- The number of inspection times in buildings will be increased due to the ease and low cost of the system.
2- This study will be fundamentally important in the world of sensing, artificial intelligence, and the automation of non-destructive inspection.

5.2   Future work

Estimating void size

The void area size in the experiment was based on tile size. Therefore, the area of the tile was assumed to be 100% because the hammering test and conventional method were performed in units of tiles. The tile and void sheet have the same rectangular shape; thus, the area of the void was measured with respect to the area of the tile in this study. In future studies, the shape of the void will be made more realistic. The accuracy of the void information should be improved by developing a methodology that establishes the trend data. We focused on the possibility of creating a mathematical model for the reflections from voids on tiles. Experiments were conducted on a sample in a standard case because the study was an introductory study. However, various external influences exist, e.g., moisture and dust on the surfaces of the tiles and water in the case of rain. These will be addressed in future studies.

Optimizing the number of scan layers

In the future, we will first focus on making scanning more practical by determining the magnitude of the effect of d_v value on δE and using simulations based on the mathematical models for E_T and E_v. We will follow this up by conducting an actual scan on defective tiles, including using different d_v values. In this experiment, the changes in the dielectric constant due to humidity were not considered in the simulation or experiment. The concrete in the study was in a standard state and thus a fixed dielectric constant was used assumed. In future studies, the change in the dielectric constant will be considered in the simulations, and further experiments will be conducted on concrete under different humidity conditions.

Research achievements

Peer-reviewed papers published in academic journals

- 1)Alsalem, Hussain, Takayuki Tanaka, Takumi Honda, Satoru Doi, Shigeru Uchida, and Wakuto Ono. "Measurement of the Void Size Between Wall Tiles and Concrete Through non-destructive Inspection Using Electromagnetic Waves." IEEJ Transactions on Electrical and Electronic Engineering (2022).

Peer-reviewed papers presented at international conferences

- 1) Alsalem, H., Tanaka, T., Honda, T., Doi, S., and Uchida, S. (2020). Measuring Adhesion Strength of Wall Tile to Concrete by non-Contact inspection Using Electromagnetic Waves. In ISARC. Proceedings of the International Symposium on Automation and Robotics in Construction (Vol. 37, pp. 633-638). IAARC Publications.

- 2) Hussain Alsalem, Takayuki Tanaka, Takumi Honda, Satoru Doi, Shigeru Uchida, Wakuto Ono. "Optimizing the number of scan layers in multi-layered scanning methods for detecting void sizes in concrete building tiles using electromagnetic waves." [Manuscript submitted for publication The 2023 IEEE/SICE International Symposium on System Integrations (SII 2023) in Aug 2022. Accepted].

Acknowledgements

References

[1] Mario F. Cosmes-López, Francisco Castellanos, Prisciliano F. de J. Cano-Barrita, "Ultrasound frequency analysis for identification of aggregates and cement paste in concrete," Ultrasonics., Vol.73, No.3, pp. 88-95, 2017, https://doi.org/10.1016/j.ultras.2016.08.016

[2] Rucka, Magdalena and Wilde, Krzysztof, "Ultrasound monitoring for evaluation of damage in reinforced concrete," Bulletin of the Polish Academy of Sciences. Technical Sciences., Vol.63, No.1, pp., 2015, DOI:10.1515/bpasts-2015-0008

[3] Schickert, Martin, "Progress in ultrasonic imaging of concrete," Materials and Structures, Vol.38, No.9 (2005), DOI:10.1007/BF02481653

[4] Kim, Yoo Jin and Jofre, Luis and De Flaviis, Franco and Feng, Maria Q, "Microwave reflection tomographic array for damage detection of civil structures," IEEE Transactions on Antennas and Propagation, Vol.51, No.11(2003) 3022-3032, DOI:10.1109/TAP.2003.818786

[5] Salvad, Andrea and Pastorino, Matteo and Monleone, Ricardo and Bartesaghi, Thomas and Bozza, Giovanni and Randazzo, Andrea, "Microwave detection of dielectric structures by using a tomographic approach," 2008 IEEE Instrumentation and Measurement Technology Conference, (2008) 1300-1305, DOI: 10.1109/IMTC.2008.4547243

[6] Foudazi, Ali and Mehdipour, Iman and Donnell, Kristen M and Khayat, Kamal H, "Evaluation of steel fiber distribution in cement-based mortars using active microwave thermography," Materials and Structures, Vol.49, No. 12 (2016) 5051-5065, DOI:10.1109/I2MTC.2018.8409631

[7] • Zoughi R and Bakhtiari Sasan, "Microwave non-destructive detection and evaluation of voids in layered dielectric slabs," Research in Nondestructive Evaluation., Vol.2, No.4, pp. 195-205, 1990, DOI:https://doi.org/10.1007/BF01626079

[8] Al-Qadi, Imad L and Ghodgaonkar, Deepak K and Varada, Vijay K and Varadan, Vasundara V, "Effect of moisture on asphaltic concrete at microwave frequencies," IEEE Transactions on Geoscience and Remote sensing., Vol.29, No.5, pp. 710-717, 1991, DOI: 10.1109/TGRS.1991.817705

[9] TANAKA, Shogo and YAMADA, Minoru, "Non-destructive inspection of concrete structures using an electromagnetic wave (radar) based on a signal propagation model," Transactions of the Society of Instrument and Control Engineers., Vol.39, No.5, pp. 432-440, 2003,DOI: https://doi.org/10.9746/sicetr1965.39.432

[10] Chen, Guanren and Katagiri, Takuya and Song, Haicheng and Yusa, Noritaka and Hashizume, Hidetoshi, "Investigation of the effect of a bend on pipe inspection using

microwave NDT," NDT and E International., Vol.110, No.3, pp. 102-208, 2020,DOI: https://doi.org/10.1016/j.ndteint.2019.102208

[11] Sasaki, Kota and Katagiri, Takuya and Yusa, Noritaka and Hashizume, Hidetoshi, "Demonstration of the applicability of non-destructive microwave testing to the long-range inspection of inner-surface cracks in tubes," Materials Transactions., Vol.58, No.4, pp. 692-696, 2017,DOI: https://doi.org/10.2320/matertrans.M2017008

[12] Feng, Maria Q and De Flaviis, Franco and Kim, Yoo Jin, "Use of microwaves for damage detection of fiber reinforced polymer-wrapped concrete structures," Journal of Engineering Mechanics., Vol.128, No.2, pp. 172-183,2002,DOI: https://doi.org/10.1061/(ASCE)0733-9399(2002)128:2(172)

[13] Kim, Yoo Jin and Jofre, Luis and De Flaviis, Franco and Feng, Maria Q, "Microwave cylindrical reflection imaging array for structural damage detection," IEEE Antennas and Propagation Society International Symposium., Vol.2, No.3, pp. 678-681, 2001, DOI: 10.1109/APS.2001.959815

[14] Honda, Takumi and Tanaka, Takayuki and Doi, Satoru and Uchida, Shigeru and Feng, Maria Q, "Visualization of voids between tile and concrete by multi-layered scanning method with electromagnetic waves," Journal of Robotics and Mechatronics., Vol.31, No.6, pp. 863-870, 2019,DOI: https://doi.org/10.20965/jrm.2019.p0863

[15] Kawataki, Shotaro and Tanaka, Takayuki and Doi, Satoru and Uchida, Shigeru and Feng, Maria Q, "Non-destructive inspection of voids in concrete by multi-layered scanning method with electromagnetic waves," 2017 IEEE International Conference on Mechatronics (ICM)., pp. 336-341, 2017, DOI: 10.1109/ICMECH.2017.7921127

[16] Chew, M. Y. L, "Factors affecting ceramic tile adhesion for external cladding," Construction and Building Materials 13, no. 5 (1999): 293-296.,DOI: https://doi.org/10.1016/S0950-0618(99)00023-9

[17] Ramos, NMM and Simões, M Lurdes and Delgado, JMPQ and De Freitas, VP, "Reliability of the pull-off test for in situ evaluation of adhesion strength," Vol.31, No.5, pp. 86-93, 2021,DOI: https://doi.org/10.1016/j.conbuildmat.2011.12.097

[18] Wetzel, A., M. Herwegh, R. Zurbriggen, and F. Winnefeld, "Influence of shrinkage and water transport mechanisms on microstructure and crack formation of tile adhesive mortars," Cement and concrete research 42, no. 1 (2012): 39-50.,DOI: https://doi.org/10.1016/j.cemconres.2011.07.007

[19] Walsh, J., and E. W. Gill, "An analysis of the scattering of high-frequency electromagnetic radiation from rough surfaces with application to pulse radar operating in backscatter mode," Radio Science 35, no. 6 (2000): 1337-1359., DOI: 10.1029/2000RS002532

[20] Davies, H, "The reflection of electromagnetic waves from a rough surface," Proceedings of the IEE-Part IV: Institution Monographs 101, no. 7 (1954): 209-214., DOI: 10.1049/pi-4.1954.0025

[21] Batrakov, Dmitry O., Mariya S. Antyufeyeva, Alexandr V. Antyufeyev, and Angelika G. Batrakova, "GPR data processing for evaluation of the subsurface cracks in road pavements,"

In 2017 9th international workshop on advanced ground penetrating radar (IWAGPR), pp. 1-6. IEEE, 2017., DOI: 10.1109/IWAGPR.2017.7996072

[22] Meola, Carosena, "A new approach for estimation of defects detection with infrared thermography," Materials Letters 61, no. 3 (2007): 747-750,DOI: https://doi.org/10.1016/j.matlet.2006.04.120

[23] Santos-Assunçao, Sonia, Vega Perez-Gracia, Oriol Caselles, Jaume Clapes, and Victor Salinas, "Assessment of complex masonry structures with GPR compared to other non-destructive testing studies," Remote Sensing 6, no. 9 (2014): 8220-8237.,DOI: https://doi.org/10.3390/rs6098220

[24] Iyer, Shivprakash, Sunil K. Sinha, Bernhard R. Tittmann, and Michael K. Pedrick. "Ultrasonic signal processing methods for detection of defects in concrete pipes." Automation in Construction 22 (2012): 135-148.,DOI: https://doi.org/10.1016/j.autcon.2011.06.012

[25] Yang, Jun, Wei Wang, Guang Lin, Qing Li, Yeqing Sun, and Yixuan Sun, "Infrared thermal imaging-based crack detection using deep learning," IEEE Access 7 (2019): 182060-182077. DOI: 10.1109/ACCESS.2019.2958264

[26] Feng, M. Q., Kim, Y. J., and Park, K, "Real-Time and Hand-Held Microwave NDE Technology for Inspection of FRP-Wrapped Concrete Structures," FRP International-The Official Newsletter of the International Institute for FRP in Construction, 3(2), 2-5, 2006., doi: 10.20965/jrm.2019.p0863

[27] Feng, M. Q. (2007). Smart Array Antenna for NDE of FRP-Wrapped Concrete Bridge Members (No. TRB-NCHRP-109)., DOI:10.1016/j.conbuildmat.2007.09.009

[28] Muehldorf, E., "The phase center of horn antennas, " IEEE Transactions on Antennas and Propagation 18, no. 6 (1970): 753-760., DOI: 10.1109/TAP.1970.1139799

[29] Alsalem, Hussain, Takayuki Tanaka, Takumi Honda, Satoru Doi, Shigeru Uchida, and Wakuto Ono. "Measurement of the Void Size Between Wall Tiles and Concrete Through Nondestructive Inspection Using Electromagnetic Waves." IEEJ Transactions on Electrical and Electronic Engineering (2022).DOI: https://doi.org/10.1002/tee.23755

[30] Alsalem, Hussain, Takayuki Tanaka, Takumi Honda, Satoru Doi, and Shigeru Uchida. "Measuring Adhesion Strength of Wall Tile to Concrete by Non-Contact Inspection Using Electromagnetic Waves." In ISARC. Proceedings of the International Symposium on Automation and Robotics in Construction, vol. 37, pp. 633-638. IAARC Publications, 2020., DOI: https://doi.org/10.22260/ISARC2020/0088

[31] Takumi Honda, Takayuki Tanaka, Satoru Doi, Shigeru Uchida, and Maria Q. Feng, "Visualization of Voids Between Tile and Concrete by Multi- Layered Scanning Method with Electromagnetic Waves, " Journal of Robotics and Mechatronics (JRM) Vol.31 No.6 pp. 863-870, 2019, DOI: https://doi.org/10.20965/jrm.2019.p0863

[32] Kawataki. S, Tanaka. T, Doi. S, Uchida. S, and Feng. M. Q, "Nondestructive In-spection of Voids in Concrete by Multi-layered Scanning Method with Electro-magnetic Waves, " Proc. of the IEEE International Conference on MECHA-TRONICS (IEEE-ICM2017), pp.336-341, 2017., DOI: 10.1109/ICMECH.2017.7921127